Inorganic Chemistry

Article

pubs.acs.org/IC

Supramolecular β-Cyclodextrin Adducts of Boron-Rich DNA Metallointercalators Containing Dicarba-*closo*-dodecaborane(12)

H. Y. Vincent Ching, Ronald J. Clarke, and Louis M. Rendina*

School of Chemistry, The University of Sydney, Sydney, NSW 2006, Australia

Supporting Information

ABSTRACT: A chiral, isomeric series of novel boron-rich Pt^{II} metallointercalators ($[PtL_2(phen)](NO_3)_2$: L = (**x**)-(1,**y**-*closo*-carboran-1-yl)pyrid-**z**-ylmethanol: **x** = *R*, *S*; **y** = 7, 12; **z** = 3, 4) wre prepared and fully characterized. By means of variable-temperature NMR spectroscopy, different combinations of Δ-head-to-tail, head-to-head, and Λ-head-to-tail rotamers were identified, and the free energies of activation for Pt−N bond rotation were determined for the pyrid-4-yl complexes with $\Delta G^{\ddagger}_{307} = 16.1 \pm 0.3$ kcal mol^{-1} and $\Delta G^{\ddagger}_{325} = 16.2 \pm 0.5$ kcal mol^{-1} for the 1,7-carboranyl derivative and $\Delta G^{\ddagger}_{307} = 16.4 \pm 0.5$ kcal mol^{-1} and $\Delta G^{\ddagger}_{325} = 16.2 \pm 0.5$ kcal mol^{-1} for the 1,12-carboranyl derivative. The corresponding 2:1 host−guest β-cyclodextrin (β-CD) adducts ($[PtL_2(phen)\cdot 2\beta\text{-CD}](NO_3)_2$) were also prepared and fully characterized by high resolution electrospray ionization mass spectrometry and 2D-$^1H\{^{11}B\}$ nuclear Overhauser enhancement spectroscopy and rotating-frame Overhauser effect spectroscopy NMR experiments. The interaction of the novel supramolecular adducts with calf thymus DNA was investigated by means of linear dichroism, ultraviolet-visible spectroscopy, thermal denaturation, and isothermal titration calorimetry experiments which revealed a bimodal binding regime with DNA intercalation favored at low [drug]/[DNA] ratios, while at higher drug loading, surface aggregation was observed. Furthermore, the data were also consistent with some degree of dissociation of the β-CD host−guest adducts upon DNA binding. When we used a single binding-site model, interpreted as a weighted average of all of the possible equilibrium interactions, the compounds showed high affinity for ct-DNA with K_{assoc} ranging from $(1.3 \pm 0.1) \times 10^5$ M^{-1} to $(5.7 \pm 0.4) \times 10^5$ M^{-1}. In general, the overall DNA-binding behavior was enthalpically driven with a minor or unfavorable entropic component, which is consistent with the thermodynamics of an intercalation-dominated process. A higher degree of DNA intercalation was observed for the *R*-isomer in the pyrid-3-yl compounds, and the opposite trend was observed in the case of pyrid-4-yl derivatives.

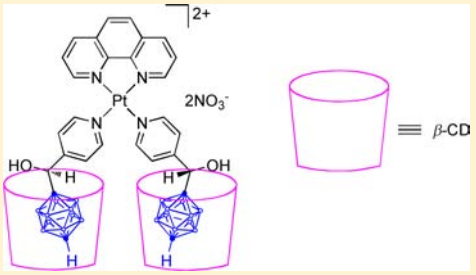

INTRODUCTION

Since the pioneering work on cationic, square-planar Pt^{II} complexes containing 2,2′:6′,2″-terpyridine (terpy) by Lippard and co-workers,[1] DNA-metallointercalators have been widely studied, and their application as biomolecular probes and potential chemotherapeutic agents is now well-established.[2] Chromosomal DNA is an important drug target for the binary cancer treatment boron neutron capture therapy (BNCT), and numerous strategies have been investigated for the delivery of large numbers of boron atoms to this critical macromolecule.[3] Previously, a series of Pt^{II}(terpy) complexes containing thioalkylcarborane ligands were reported as a new class of potential BNCT agents.[4] Preliminary biological assessments have shown promising in vitro antitumor activity, but the high lipophilicity of the boron clusters limited the bioavailability of these agents. A more hydrophilic derivative, containing a pendant glycerol moiety, has also been prepared, but its synthesis is lengthy and highly involved.[5]

Lipophilic drugs have often been solubilized by the formation of supramolecular host−guest adducts with β-cyclodextrin (homochiral cyclic oligosaccharides of 1,4-α-linked D-glucose units, CD).[6] Indeed, very robust adducts of β-cyclodextrin (β-CD) or its derivatives and *closo*-carborane compounds have been demonstrated previously,[7] and the use of β-CDs as biodelivery agents for carborane clusters is of particular relevance to their exploitation as unique hydrophobic pharmacophores in medicinal chemistry.[8] Recently, we reported the β-CD encapsulation of a chiral isomeric series of Pt^{II}(terpy) complexes containing pyridylcarboranylmethanol ligands,[9] and for one of these metal complexes a remarkably stable ternary system was observed in aqueous solution involving simultaneous DNA metallointercalation and β-CD encapsulation.[10] Herein we describe the synthesis and complete characterization of a related series of chiral, boron-rich Pt^{II} DNA-metallointercalators containing two *closo*-carborane clusters which are capable of delivering 20 boron atoms per molecule to the macromolecule. To increase the aqueous solubility and bioavailability of these complexes, corresponding β-CD 2:1 host−guest adducts were also prepared in which the two lipophilic boron cages are each encapsulated by a cyclic sugar. The interactions of the host−guest adducts with calf thymus-DNA (ct-DNA) were investigated by means of linear dichroism (LD), ultraviolet-visible (UV−vis) spectrophotom-

Received: April 28, 2013
Published: August 28, 2013

   dx.doi.org/10.1021/ic401060k | *Inorg. Chem.* 2013, 52, 10356−10367

etry, DNA thermal denaturation, and isothermal titration calorimetry (ITC), which confirmed DNA intercalation but also revealed a secondary DNA-binding mode.

EXPERIMENTAL SECTION

General. High resolution electrospray ionization mass spectrometry (HR-ESI-MS) were recorded on a Bruker 7T Fourier transform ion cyclotron resonance (FTICR) mass spectrometer in the positive ESI mode. Elemental analysis was performed by Campbell Microanalytical Laboratory, Chemistry Department, The University of Otago, Dunedin, New Zealand. Commercially available deuterated solvents of 99.5% isotopic purity or higher were used for all NMR spectra. All NMR spectra were recorded at 300 K unless otherwise stated on a Bruker AVANCE DRX 400 MHz spectrometer (^{1}H at 400 MHz, ^{13}C at 101 MHz, ^{11}B at 128 MHz, and ^{195}Pt at 85 MHz). All NMR signals are reported in ppm. ^{1}H, ^{1}H{^{11}B}, and ^{13}C{^{1}H} NMR spectra were referenced to TMS (0 ppm), except for the spectra in D_2O which were referenced to trimethylsilyl propanoic acid (TSP) (0 ppm). ^{11}B{^{1}H} NMR spectra were referenced to an external standard of $BF_3{\cdot}OEt_2$ (0 ppm). ^{195}Pt NMR spectra were referenced to an external standard of $K_2[PtCl_4]$ with KCl in D_2O (−1628 ppm). ^{1}H{^{11}B} nuclear Overhauser enhancement spectroscopy (NOESY) spectra were recorded with 4096 points in t_2 for 256 t_1 values with a pulse repetition delay of 1.5 s and a mixing time of 300 ms. ^{1}H{^{11}B} rotating-frame Overhauser effect spectroscopy (ROESY) spectra were recorded with 4096 points in t_2 for 512 t_1 values with a pulse repetition delay of 2 s. Coupling constants (^nJ [ij]) are reported in Hz. Peak multiplicities have been abbreviated as s (singlet), d (doublet), t (triplet), q (quartet), m (multiplet, unassignable multiplicity, or overlapping signals), and b (broad). Selected NMR characterizations are reported herein, while the remainder are documented in the Supporting Information.

Materials. Milli-Q water was used for all experiments requiring water, and all other solvents were used without further purification. The two *closo*-carborane isomers, 1,7-$C_2H_{12}B_{10}$ and 1,12-$C_2H_{12}B_{10}$, were obtained from Katchem Pty Ltd. (Czech Republic). Potassium tetrachloridoplatinate(II) was kindly loaned from Johnson Matthey. [PtI_2(phen)] was synthesized by following the method of Wimmer and Castan.[11] The synthesis and characterization of the ligands *R*/*S*-**L**$^{1-4}$ were previously reported.[9,10] All other reagents were purchased from Sigma Aldrich and were used without further purification.

Synthesis of (*R*/*S*)-(1−4)·2NO$_3$. Unless otherwise stated, **L**$^{1-4}$ (110 mg, 0.44 mmol) was dissolved in acetonitrile (70 mL), and [PtI_2(phen)] (100 mg, 0.16 mmol) was added to the solution at 80 °C. With vigorous stirring, a solution of silver nitrate (53 mg, 0.31 mmol) in acetonitrile (5 mL) was added dropwise to the reaction mixture. After 15 min, the hot mixture was filtered through Celite filter-aid. Removal of the solvent in vacuo, followed by washing with hot dichloromethane(DCM) (3 × 10 mL), gave the desired products as crystalline solids. Unreacted pyridyl ligand was recovered from the DCM washings and was purified by filtration through a plug of silica by eluting with EtOAc.

*(R)-**1**·2NO$_3$ was prepared from (R)-**L**^{1} (colorless powder, 85 mg, 51%).* Three rotamers in a 5:4:1 ratio were observed in the NMR spectra and are denoted ***A***, ***B***, and ***C***, respectively. Rotamer ***A***: ^{1}H NMR (methanol-d_4) δ: 9.37 (d, ^3J [$H5_{py}$, $H6_{py}$] = 5.6 Hz, 2H, $H6_{py}$), 9.22 (m, 2H, $H2_{py}$), 9.07 (m, 2H, $H4_{phen}$, $H7_{phen}$), 8.34 (s, 2H, $H5_{phen}$, $H6_{phen}$), 8.27 (d, ^3J [$H4_{py}$, $H5_{py}$] = 8.1 Hz, 2H, $H4_{py}$), 8.10 (m, 2H, $H2_{phen}$, $H9_{phen}$), 8.00 (m, 2H, $H3_{phen}$, $H8_{phen}$), 7.89 (dd, ^3J [$H4_{py}$, $H5_{py}$] = 8.1 Hz, ^3J [$H5_{py}$, $H6_{py}$] = 5.6 Hz, 2H, $H5_{py}$), 5.18 (s, 2H, methine), 3.51 (bs, 2H, $H7_{CB}$), 3.0−1.3 (m, 20H, BH_{CB}). ^{13}C{^{1}H} NMR (methanol-d_4) δ: 153.5 (2C, $C6_{py}$), 152.4 (2C, $C2_{py}$), 151.9 (2C, $C2_{phen}$, $C9_{phen}$), 148.9 (2C, $C11_{phen}$, $C12_{phen}$), 144.2 (2C, $C3_{py}$), 143.0 (2C, $C4_{phen}$, $C7_{phen}$), 140.9 (2C, $C4_{py}$), 132.7 (2C, $C13_{phen}$, $C14_{phen}$), 129.8 (2C, $C5_{py}$), 129.6 (2C, $C5_{phen}$, $C6_{phen}$), 127.7 (2C, $C3_{phen}$, $C8_{phen}$), 83.0 (2C, $C1_{CB}$), 71.9 (2C, methine), 56.8 (2C, $C7_{CB}$). ^{11}B{^{1}H} NMR (methanol-d_4) δ: −7.4 (2B), −13.1 (6B), −15.3 (8B), −17.8 (4B). ^{195}Pt NMR (methanol-d_4) δ: −2536. Rotamer ***B***: ^{1}H NMR (methanol-d_4) δ: 9.40 (d, ^3J [$H5_{py}$, $H6_{py}$] = 5.6 Hz, 2H, $H6_{py}$), 9.35 (m, 2H, $H2_{py}$), 9.07 (m, 2H, $H4_{phen}$, $H7_{phen}$), 8.35 (s, 2H, $H5_{phen}$, $H6_{phen}$), 8.10 (m, 2H, $H2_{phen}$, $H9_{phen}$), 8.09 (m, 2H, $H4_{py}$), 8.00 (m, 2H, $H3_{phen}$, $H8_{phen}$), 7.84 (dd, ^3J [$H4_{py}$, $H5_{py}$] = 8.1 Hz, ^3J [$H5_{py}$, $H6_{py}$] = 5.6 Hz, 2H, $H5_{py}$), 5.19 (s, 2H, methine), 3.51 (bs, 2H, $H7_{CB}$), 3.0−1.3 (m, 20H, BH_{CB}). ^{13}C{^{1}H} NMR (methanol-d_4) δ: 153.3 (2C, $C6_{py}$), 152.4 (2C, $C2_{py}$), 151.8 (2C, $C2_{phen}$, $C9_{phen}$), 148.9 (2C, $C11_{phen}$, $C12_{phen}$), 144.3 (2C, $C3_{py}$), 143.1 (2C, $C4_{phen}$, $C7_{phen}$), 141.6 (2C, $C4_{py}$), 132.8 (2C, $C13_{phen}$, $C14_{phen}$), 129.6 (2C, $C5_{phen}$, $C6_{phen}$), 129.1 (2C, $C5_{py}$), 127.7 (2C, $C3_{phen}$, $C8_{phen}$), 82.8 (2C, $C1_{CB}$), 72.6 (2C, methine), 56.8 (2C, $C7_{CB}$). ^{11}B{^{1}H} NMR (methanol-d_4) δ: −7.4 (2B), −13.1 (6B), −15.3 (8B), −17.8 (4B). ^{195}Pt NMR (methanol-d_4) δ: −2535. Rotamer ***C***: ^{1}H NMR (methanol-d_4) δ: 9.22 (m, 2H, $H2_{py}$, $H6_{py}$), 9.07 (m, 2H, $H4_{phen}$, $H7_{phen}$), 8.37 (s, 2H, $H5_{phen}$, $H6_{phen}$), 8.23 (2H, $H4_{py}$), 8.10 (m, 2H, $H2_{phen}$, $H9_{phen}$), 8.00 (m, 2H, $H3_{phen}$, $H8_{phen}$), 7.84 (m, 2H, $H5_{py}$), 5.17 (s, 2H, methine), 3.51 (bs, 2C, $H2_{CB}$), 3.0−1.3 (m, 20H, BH_{CB}). ^{13}C{^{1}H} NMR (methanol-d_4) δ: 153.8 (2C, $C6_{py}$), 152.4 (2C, $C2_{py}$), 151.5 (2C, $C2_{phen}$, $C9_{phen}$), 148.9 (2C, $C11_{phen}$, $C12_{phen}$), 144.2 (2C, $C3_{py}$), 143.2 (2C, $C4_{phen}$, $C7_{phen}$), 141.5 (2C, $C4_{py}$), 132.84 (2C, $C13_{phen}$, $C14_{phen}$), 129.6 (2C, $C5_{phen}$, $C6_{phen}$), 129.3 (2C, $C5_{py}$), 127.7 (2C, $C3_{phen}$, $C8_{phen}$), 82.8 (2C, $C1_{CB}$), 72.2 (2C, methine), 56.8 (2C, $C7_{CB}$). ^{11}B{^{1}H} NMR (methanol-d_4) δ: −7.4 (2B), −13.1 (6B), −15.3 (8B), −17.8 (4B). ^{195}Pt NMR (methanol-d_4) δ: −2513. HR-ESI-MS Calcd for [M − 2NO_3^-]$^{2+}$, $C_{28}H_{42}B_{20}N_4O_2Pt$: *m*/*z* 439.24653. Found *m*/*z* 439.24647. Anal. Calcd for $C_{28}H_{42}B_{20}N_6O_8Pt{\cdot}2.5H_2O$: C, 32.12; H, 4.52; N, 8.03. Found: C, 31.86; H, 4.13; N, 8.07.

*(S)-**1**·2NO$_3$ was prepared from (S)-**L**^{1} (colorless powder, 78 mg, 47%).* HR-ESI-MS Calcd for [M − 2NO_3^-]$^{2+}$, $C_{28}H_{42}B_{20}N_4O_2Pt$: *m*/*z* 439.24653. Found *m*/*z* 439.24655. Anal. Calcd for $C_{28}H_{42}B_{20}N_6O_8Pt{\cdot}2H_2O$: C, 32.40; H, 4.47; N, 8.10. Found: C, 32.14; H, 4.29; N, 8.05.

*(R)-**2**·2NO$_3$ was prepared from (R)-**L**^{2} (white powder, 98 mg, 60%).* Two rotamers in a 1:1 ratio were observed in the NMR spectra and are denoted as ***A*** and ***B***, respectively. Rotamer ***A***: ^{1}H NMR (methanol-d_4) δ: 9.24 (m, 4H, $H2_{py}$), 9.08 (d, ^3J [$H3_{phen}$, $H4_{phen}$] = 8.1 Hz, 2H, $H4_{phen}$, $H7_{phen}$), 8.36 (s, 2H, $H5_{phen}$, $H6_{phen}$), 8.05 (m, 4H, $H2_{phen}$, $H3_{phen}$, $H8_{phen}$, $H9_{phen}$), 7.75 (m, 4H, $H3_{py}$), 5.16 (s, 2H, methine), 3.51 (bs, 2H, $H7_{CB}$), 3.0−1.3 (m, 20H, BH_{CB}). ^{13}C{^{1}H} NMR (methanol-d_4) δ: 158.0 (2C, $C4_{py}$), 153.9 (4C, $C2_{py}$), 151.8 (2C, $C2_{phen}$, $C9_{phen}$), 148.8 (2C, $C11_{phen}$, $C12_{phen}$), 143.1 (2C, $C4_{phen}$, $C7_{phen}$), 132.7 (2C, $C13_{phen}$, $C14_{phen}$), 129.6 (2C, $C5_{phen}$, $C6_{phen}$), 127.7 (2C, $C3_{phen}$, $C8_{phen}$), 127.5 (4C, $C3_{py}$), 81.9 (2C, $C1_{CB}$), 73.1 (2C, methine), 56.8 (2C, $C7_{CB}$). ^{11}B{^{1}H} NMR (methanol-d_4) δ: −3.6 (2B), −9.6 (6B), −11.8 (8B), −14.2 (4B). ^{195}Pt NMR (methanol-d_4) δ: −2519. Rotamer ***B***: ^{1}H NMR (methanol-d_4) δ: 9.22 (m, 4H, $H2_{py}$), 9.08 (dd, ^3J [$H3_{phen}$, $H4_{phen}$] = 8.1 Hz, 2H, $H4_{phen}$, $H7_{phen}$), 8.36 (s, 2H, $H5_{phen}$, $H6_{phen}$), 8.05 (m, 4H, $H2_{phen}$, $H3_{phen}$, $H8_{phen}$, $H9_{phen}$), 7.83 (m, 4H, $H3_{py}$), 5.16 (s, 2H, methine), 3.51 (bs, 2H, $H7_{CB}$), 3.0−1.3 (m, 20H, BH_{CB}). ^{13}C{^{1}H} NMR (methanol-d_4) δ: 158.0 (2C, $C4_{py}$), 153.6 (4C, $C2_{py}$), 151.8 (2C, $C2_{phen}$, $C9_{phen}$), 148.8 (2C, $C11_{phen}$, $C12_{phen}$), 143.1 (2C, $C4_{phen}$, $C7_{phen}$), 132.7 (2C, $C13_{phen}$, $C14_{phen}$), 129.6 (2C, $C5_{phen}$, $C6_{phen}$), 128.0 (4C, $C3_{py}$), 127.7 (2C, $C3_{phen}$, $C8_{phen}$), 81.9 (2C, $C1_{CB}$), 73.1 (2C, methine), 56.8 (2C, $C7_{CB}$). ^{11}B{^{1}H} NMR (methanol-d_4) δ: −3.6 (2B), −9.6 (6B), −11.8 (8B), −14.2 (4B). ^{195}Pt NMR (methanol-d_4) δ: −2518. HR-ESI-MS Calcd for [M − 2NO_3^-]$^{2+}$, $C_{28}H_{42}B_{20}N_4O_2Pt$: *m*/*z* 439.24653. Found *m*/*z* 439.24648. Anal. Calcd for $C_{28}H_{42}B_{20}N_6O_8Pt{\cdot}H_2O$: C, 32.97; H, 4.35; N, 8.24. Found: C, 32.56; H, 4.21; N, 8.38.

*(S)-**2**·2NO$_3$ was prepared from (S)-**L**^{2} (colorless powder, 130 mg, 80%).* HR-ESI-MS Calcd for [M − 2NO_3^-]$^{2+}$, $C_{28}H_{42}B_{20}N_4O_2Pt$: *m*/*z* 439.24653. Found *m*/*z* 439.24624. Anal. Calcd for $C_{28}H_{42}B_{20}N_6O_8Pt{\cdot}H_2O$: C, 32.97; H, 4.35; N, 8.24. Found: C, 32.70; H, 4.25; N, 8.31.

*(R)-**3**·2NO$_3$ was prepared from (R)-**L**^{3}.* The crude product was washed with hot acetone instead of DCM (pale yellow powder, 100 mg, 63%). Please see Supporting Information for complete NMR characterizations. HR-ESI-MS Calcd for [M − 2NO_3^-]$^{2+}$, $C_{28}H_{42}B_{20}N_4O_2Pt$: *m*/*z* 439.24653. Found *m*/*z* 439.24593. Anal. Calcd for $C_{28}H_{42}B_{20}N_6O_8Pt$: C, 33.56; H, 4.23; N, 8.39. Found: C, 33.58; H, 4.29; N, 8.32.

*(S)-**3**·2NO$_3$ was prepared from (S)-**L**^{3}.* The crude product was washed with hot acetone instead of DCM (pale yellow powder, 120

dx.doi.org/10.1021/ic401060k | Inorg. Chem. 2013, 52, 10356−10367

mg, 74%). HR-ESI-MS Calcd for $[M - 2NO_3^-]^{2+}$, $C_{28}H_{42}B_{20}N_4O_2Pt$: m/z 439.24653. Found m/z 439.24645. Anal. Calcd for $C_{28}H_{42}B_{20}N_6O_8Pt$: C, 33.56; H, 4.23; N, 8.39. Found: C, 33.16; H, 4.07; N, 8.06.

*(R)-**4**·2NO$_3$ was prepared from (R)-**L**^{4}.* The crude product was washed with hot acetone instead of DCM (pale yellow powder, 100 mg, 63%). Please see Supporting Information for complete NMR characterizations. HR-ESI-MS Calcd for $[M - 2NO_3^-]^{2+}$, $C_{28}H_{42}B_{20}N_4O_2Pt$: m/z 439.24653. Found m/z 439.24618. Anal. Calcd for $C_{28}H_{42}B_{20}N_6O_8Pt$: C, 33.56; H, 4.23; N, 8.39. Found: C, 33.81; H, 4.28; N, 8.38.

*(S)-**4**·2NO$_3$ was prepared from (S)-**L**^{4}.* The crude product was washed with hot acetone instead of DCM (pale yellow powder, 100 mg, 63%). HR-ESI-MS Calcd for $[M - 2NO_3^-]^{2+}$, $C_{28}H_{42}B_{20}N_4O_2Pt$: m/z 439.24653. Found m/z 439.24624. HR-ESI-MS Calcd for $[M - H_2O - 2NO_3^-]^{2+}$, $C_{28}H_{42}B_{20}N_4O_2Pt$: m/z 439.24653. Found m/z 439.24593. Anal. Calcd for $C_{28}H_{42}B_{20}N_6O_8Pt$: C, 33.56; H, 4.23; N, 8.39. Found: C, 33.47; H, 4.20; N, 8.27.

Synthesis of (*R/S*)-(1−4)·2*β*-CD·2NO$_3$. (*R/S*)-(1−4)·2NO$_3$ (5.00 μmol) was suspended in a 2.0 mM aqueous solution of *β*-CD (5.0 mL, 10.00 μmol) and sonicated for 30 min, or until the solution became clear. Filtration through cellulose followed by lyophilization gave the desired product as a white powder.

*(R)-**1**·2β-CD·2NO$_3$ was prepared from (R)-**1**·2NO$_3$ (17 mg, quantitative).* Two major rotamers in a 2:1 ratio were observed and are denoted as ***A*** and ***B***, respectively. Rotamer ***A***: ^{1}H NMR (D_2O) δ: 9.34 (m, 2H, $H6_{py}$), 8.97 (m, 2H, $H2_{py}$), 8.88 (m, 2H, $H4_{phen}$, $H7_{phen}$), 8.31 (m, 2H, $H4_{py}$), 8.19 (m, 2H, $H5_{phen}$, $H6_{phen}$), 8.10 (m, 2H, $H2_{phen}$, $H9_{phen}$), 8.02 (m, 2H, $H5_{py}$), 7.85 (m, 2H, $H3_{phen}$, $H8_{phen}$), 5.14 (m, 2H, methine), 4.97 (d, ^3J [$H1_{β\text{-CD}}$, $H2_{β\text{-CD}}$] = 3.4 Hz, 14H, $H1_{β\text{-CD}}$), 3.96 (dd, ^3J [$H2_{β\text{-CD}}$, $H3_{β\text{-CD}}$] = 9.5 Hz, ^3J [$H3_{β\text{-CD}}$, $H4_{β\text{-CD}}$] = 9.5 Hz, 14H, $H3_{β\text{-CD}}$), 3.79, (m, 14H, $H6_{β\text{-CD}}$), 3.72 (m, 14H, $H5_{β\text{-CD}}$), 3.58 (dd, ^3J [$H1_{β\text{-CD}}$, $H2_{β\text{-CD}}$] = 3.4 Hz, ^3J [$H2_{β\text{-CD}}$, $H3_{β\text{-CD}}$] = 9.5 Hz, 14H, $H2_{β\text{-CD}}$), 3.51 (dd, ^3J [$H3_{β\text{-CD}}$, $H4_{β\text{-CD}}$] = 9.5 Hz, ^3J [$H4_{β\text{-CD}}$, $H5_{β\text{-CD}}$] = 9.5 Hz, 14H, $H4_{β\text{-CD}}$), 3.45 (bs, 2H, $H7_{CB}$), 3.0−1.3 (m, 20H, BH_{CB}). ^{13}C{^{1}H} NMR (D_2O) δ: 152.4 (2C, $C6_{py}$), 150.6 (2C, $C2_{py}$), 150.5 (2C, $C2_{phen}$, $C9_{phen}$), 147.6 (2C, $C11_{phen}$, $C12_{phen}$), 142.1 (2C, $C3_{py}$), 141.9 (2C, $C4_{phen}$, $C7_{phen}$), 139.4 (2C, $C4_{py}$), 131.2 (2C, $C13_{phen}$, $C14_{phen}$), 129.5 (2C, $C5_{py}$), 128.2 (2C, $C5_{phen}$, $C6_{phen}$), 126.0 (2C, $C3_{phen}$, $C8_{phen}$), 102.3 (14C, $C1_{β\text{-CD}}$), 81.7 (14C, $C4_{β\text{-CD}}$), 80.8 (2C, $C1_{CB}$), 73.2 (14C, $C3_{β\text{-CD}}$), 72.0 (14C, $C2_{β\text{-CD}}$), 71.8 (14C, $C5_{β\text{-CD}}$), 71.2 (2C, methine), 60.2 (14C, $C6_{β\text{-CD}}$), 55.8 (2C, $C7_{CB}$). ^{11}B{^{1}H} NMR (D_2O) δ: −10.9 (because of inherent signal broadness, not all B resonances were observed). ^{195}Pt NMR (D_2O) δ: −2549. Rotamer ***B***: ^{1}H NMR (D_2O) δ: 9.34 (m, 2H, $H6_{py}$), 9.14 (m, 2H, $H2_{py}$), 8.88 (m, 2H, $H4_{phen}$, $H7_{phen}$), 8.19 (m, 2H, $H5_{phen}$, $H6_{phen}$), 8.10 (m, 2H, $H4_{py}$), 8.04 (m, 2H, $H2_{phen}$, $H9_{phen}$), 7.90 (m, 2H, $H5_{py}$), 7.85 (m, 2H, $H3_{phen}$, $H8_{phen}$), 5.27 (m, 2H, methine), 4.97 (d, ^3J [$H1_{β\text{-CD}}$, $H2_{β\text{-CD}}$] = 3.4 Hz, 14H, $H1_{β\text{-CD}}$), 3.96 (dd, ^3J [$H2_{β\text{-CD}}$, $H3_{β\text{-CD}}$] = 9.5 Hz, ^3J [$H3_{β\text{-CD}}$, $H4_{β\text{-CD}}$] = 9.5 Hz, 14H, $H3_{β\text{-CD}}$), 3.79, (m, 14H, $H6_{β\text{-CD}}$), 3.72 (m, 14H, $H5_{β\text{-CD}}$), 3.58 (dd, ^3J [$H1_{β\text{-CD}}$, $H2_{β\text{-CD}}$] = 3.4 Hz, ^3J [$H2_{β\text{-CD}}$, $H3_{β\text{-CD}}$] = 9.5 Hz, 14H, $H2_{β\text{-CD}}$), 3.51 (dd, ^3J [$H3_{β\text{-CD}}$, $H4_{β\text{-CD}}$] = 9.5 Hz, ^3J [$H4_{β\text{-CD}}$, $H5_{β\text{-CD}}$] = 9.5 Hz, 14H, $H4_{β\text{-CD}}$), 3.45 (bs, 2H, $H7_{CB}$), 3.0−1.3 (m, 20H, BH_{CB}). ^{13}C{^{1}H} NMR (D_2O) δ: 152.4 (2C, $C6_{py}$), 150.6 (2C, $C2_{py}$), 150.5 (2C, $C2_{phen}$, $C9_{phen}$), 147.6 (2C, $C11_{phen}$, $C12_{phen}$), 142.1 (2C, $C3_{py}$), 141.9 (2C, $C4_{phen}$, $C7_{phen}$), 139.4 (2C, $C4_{py}$), 131.2 (2C, $C13_{phen}$, $C14_{phen}$), 129.5 (2C, $C5_{py}$), 128.2 (2C, $C5_{phen}$, $C6_{phen}$), 126.0 (2C, $C3_{phen}$, $C8_{phen}$), 102.3 (14C, $C1_{β\text{-CD}}$), 81.7 (14C, $C4_{β\text{-CD}}$), 80.8 (2C, $C1_{CB}$), 73.2 (14C, $C3_{β\text{-CD}}$), 72.0 (14C, $C2_{β\text{-CD}}$), 71.8 (14C, $C5_{β\text{-CD}}$), 71.2 (2C, methine), 60.2 (14C, $C6_{β\text{-CD}}$), 55.8 (2C, $C7_{CB}$). ^{11}B{^{1}H} NMR (D_2O) δ: −10.9 (because of inherent signal broadness, not all B resonances were observed). ^{195}Pt NMR (D_2O) δ: −2549. HR-ESI-MS Calcd for $[M - 2NO_3^-]^{2+}$, $C_{112}H_{182}B_{20}N_4O_{72}Pt$: m/z 1574.11863. Found m/z 1574.11841. Anal. Calcd for $C_{112}H_{182}B_{20}N_6O_{78}Pt·15H_2O$: C, 37.98; H, 6.03; N, 2.37. Found: C, 37.71; H, 5.81; N, 2.67.

*(S)-**1**·2β-CD·2NO$_3$ was prepared from (S)-**1**·2NO$_3$ (17 mg, quantitative).* Please see Supporting Information for complete NMR characterizations. HR-ESI-MS Calcd for $[M - 2NO_3^-]^{2+}$, $C_{112}H_{182}B_{20}N_4O_{72}Pt$: m/z 1574.11863. Found m/z 1574.11904. Anal. Calcd for $C_{112}H_{182}B_{20}N_6O_{74}Pt·15H_2O$: C, 37.98; H, 6.03; N, 2.37. Found: C, 37.64; H, 5.70; N, 2.79.

*(R)-**2**·2β-CD·2NO$_3$ was prepared from (R)-**2**·2NO$_3$ (17 mg, quantitative).* Two rotamers in a 1:1 population ratio were observed and are denoted as ***A*** and ***B***, respectively. Rotamer ***A***: ^{1}H NMR (D_2O, 320 K) δ: 9.36 (m, 4H, $H2_{py}$), 8.94 (d, ^3J [$H3_{phen}$, $H4_{phen}$] = 8.1 Hz, 2H, $H4_{phen}$, $H7_{phen}$), 8.34 (d, ^3J [$H2_{phen}$, $H3_{phen}$] = 5.6 Hz, 2H, $H2_{phen}$, $H9_{phen}$), 8.23 (s, 2H, $H5_{phen}$, $H6_{phen}$), 7.95 (dd, ^3J [$H2_{phen}$, $H3_{phen}$] = 5.6 Hz, ^3J [$H3_{phen}$, $H4_{phen}$] = 8.1 Hz, 2H, $H3_{phen}$, $H8_{phen}$), 7.94 (m, 4H, $H3_{py}$), 5.22 (s, 2H, methine), 5.02 (d, ^3J [$H1_{β\text{-CD}}$, $H2_{β\text{-CD}}$] = 3.4 Hz, 14H, $H1_{β\text{-CD}}$), 4.01 (dd, ^3J [$H2_{β\text{-CD}}$, $H3_{β\text{-CD}}$] = 9.5 Hz, ^3J [$H3_{β\text{-CD}}$, $H4_{β\text{-CD}}$] = 9.5 Hz, 14H, $H3_{β\text{-CD}}$), 3.84 (m, 14H, $H6_{β\text{-CD}}$), 3.74 (m, 14H, $H5_{β\text{-CD}}$), 3.64 (dd, ^3J [$H1_{β\text{-CD}}$, $H2_{β\text{-CD}}$] = 3.4 Hz, ^3J [$H2_{β\text{-CD}}$, $H3_{β\text{-CD}}$] = 9.5 Hz, 14H, $H2_{β\text{-CD}}$), 3.57 (dd, ^3J [$H3_{β\text{-CD}}$, $H4_{β\text{-CD}}$] = 9.5 Hz, ^3J [$H4_{β\text{-CD}}$, $H5_{β\text{-CD}}$] = 9.5 Hz, 14H, $H4_{β\text{-CD}}$), 3.41 (bs, 2H, $H7_{CB}$), 3.0−1.3 (m, 20H, BH_{CB}). ^{13}C{^{1}H} NMR (D_2O, 320 K) δ: 155.7 (2C, $C4_{py}$), 153.5 (4C, $C2_{py}$), 150.9 (2C, $C2_{phen}$, $C9_{phen}$), 147.7 (2C, $C11_{phen}$, $C12_{phen}$), 142.2 (2C, $C4_{phen}$, $C7_{phen}$), 131.4 (2C, $C13_{phen}$, $C14_{phen}$), 128.5 (2C, $C5_{phen}$, $C6_{phen}$), 126.8 (4C, $C3_{py}$), 126.4 (2C, $C3_{phen}$, $C8_{phen}$), 102.7 (14C, $C1_{β\text{-CD}}$), 82.0 (14C, $C4_{β\text{-CD}}$), 80.6 (2C, $C1_{CB}$), 73.5 (14C, $C3_{β\text{-CD}}$), 72.4 (14C, $C2_{β\text{-CD}}$), 72.1 (14C, $C5_{β\text{-CD}}$), 71.8 (2C, methine), 60.5 (14C, $C6_{β\text{-CD}}$), 56.1 (2C, $C12_{CB}$). ^{11}B{^{1}H} NMR (D_2O, 320 K) δ: −13.8, −16.0 (because of inherent signal broadness not all B resonances were observed). ^{195}Pt NMR (D_2O, 320 K) δ: −2506. Rotamer ***B***: ^{1}H NMR (D_2O, 320 K)) δ: 8.94 (d, ^3J [$H3_{phen}$, $H4_{phen}$] = 8.1 Hz, 2H, $H4_{phen}$, $H7_{phen}$), 8.43 (m, 4H, $H2_{py}$), 8.34 (d, ^3J [$H2_{phen}$, $H3_{phen}$] = 5.6 Hz, 2H, $H2_{phen}$, $H9_{phen}$), 8.23 (s, 2H, $H5_{phen}$, $H6_{phen}$), 7.95 (dd, ^3J [$H2_{phen}$, $H3_{phen}$] = 5.6 Hz, ^3J [$H3_{phen}$, $H4_{phen}$] = 8.1 Hz, 2H, $H3_{phen}$, $H8_{phen}$), 7.59 (m, 4H, $H3_{py}$), 5.22 (s, 2H, methine), 5.02 (d, ^3J [$H1_{β\text{-CD}}$, $H2_{β\text{-CD}}$] = 3.4 Hz, 14H, $H1_{β\text{-CD}}$), 4.01 (dd, ^3J [$H2_{β\text{-CD}}$, $H3_{β\text{-CD}}$] = 9.5 Hz, ^3J [$H3_{β\text{-CD}}$, $H4_{β\text{-CD}}$] = 9.5 Hz, 14H, $H3_{β\text{-CD}}$), 3.84, (m, 14H, $H6_{β\text{-CD}}$), 3.74 (m, 14H, $H5_{β\text{-CD}}$), 3.64 (dd, ^3J [$H1_{β\text{-CD}}$, $H2_{β\text{-CD}}$] = 3.4 Hz, ^3J [$H2_{β\text{-CD}}$, $H3_{β\text{-CD}}$] = 9.5 Hz, 14H, $H2_{β\text{-CD}}$), 3.57 (dd, ^3J [$H3_{β\text{-CD}}$, $H4_{β\text{-CD}}$] = 9.5 Hz, ^3J [$H4_{β\text{-CD}}$, $H5_{β\text{-CD}}$] = 9.5 Hz, 14H, $H4_{β\text{-CD}}$), 3.41 (bs, 2H, $H7_{CB}$), 3.0−1.3 (m, 20H, BH_{CB}). ^{13}C{^{1}H} NMR (D_2O, 320 K) δ: 155.7 (2C, $C4_{py}$), 152.1 (4C, $C2_{py}$), 150.9 (2C, $C2_{phen}$, $C9_{phen}$), 147.7 (2C, $C11_{phen}$, $C12_{phen}$), 142.2 (2C, $C4_{phen}$, $C7_{phen}$), 131.4 (2C, $C13_{phen}$, $C14_{phen}$), 128.5 (2C, $C5_{phen}$, $C6_{phen}$), 126.8 (4C, $C3_{py}$), 126.4 (2C, $C3_{phen}$, $C8_{phen}$), 102.7 (14C, $C1_{β\text{-CD}}$), 82.0 (14C, $C4_{β\text{-CD}}$), 80.6 (2C, $C1_{CB}$), 73.5 (14C, $C3_{β\text{-CD}}$), 72.4 (14C, $C2_{β\text{-CD}}$), 72.1 (14C, $C5_{β\text{-CD}}$), 71.8 (2C, methine), 60.5 (14C, $C6_{β\text{-CD}}$), 56.1 (2C, $C12_{CB}$). ^{11}B{^{1}H} NMR (D_2O, 320 K) δ: −13.8, −16.0 (because of inherent signal broadness not all B resonances were observed). ^{195}Pt NMR (D_2O, 320 K) δ: −2506. HR-ESI-MS Calcd for $[M - 2NO_3^-]^{2+}$, $C_{112}H_{182}B_{20}N_4O_{72}Pt$: m/z 1574.11863. Found m/z 1574.12311. Anal. Calcd for $C_{112}H_{182}B_{20}N_6O_{74}Pt·16H_2O$: C, 37.78; H, 6.06; N, 2.36. Found: C, 37.43; H, 5.75; N, 2.41.

*(S)-**2**·2β-CD·2NO$_3$ was prepared from (S)-**2**·2NO$_3$ (17 mg, quantitative).* Please see Supporting Information for complete NMR characterizations. HR-ESI-MS Calcd for $[M - 2NO_3^-]^{2+}$, $C_{112}H_{182}B_{20}N_4O_{72}Pt$: m/z 1574.11863. Found m/z 1574.11407. Anal. Calcd for $C_{112}H_{182}B_{20}N_6O_{72}Pt·15H_2O$: C, 37.98; H, 6.03; N, 2.37. Found: C, 38.01; H, 6.00; N, 2.62.

*(R)-**3**·2β-CD·2NO$_3$ was prepared from (R)-**3**·2NO$_3$ (17 mg, quantitative).* Please see Supporting Information for complete NMR characterizations. HR-ESI-MS Calcd for $[M - 2NO_3^-]^{2+}$, $C_{112}H_{182}B_{20}N_4O_{72}Pt$: m/z 1574.11863. Found m/z 1574.11288. Anal. Calcd for $C_{112}H_{182}B_{20}N_6O_{72}Pt·15H_2O$: C, 37.98; H, 6.03; N, 2.37. Found: C, 37.81; H, 5.77; N, 2.90

*(S)-**3**·2β-CD·2NO$_3$ was prepared from (S)-**3**·2NO$_3$ (17 mg, quantitative).* Please see Supporting Information for complete NMR characterizations. HR-ESI-MS Calcd for $[M - 2NO_3^-]^{2+}$, $C_{112}H_{182}B_{20}N_4O_{72}Pt$: m/z 1574.11863. Found m/z 1574.11705. Anal. Calcd for $C_{112}H_{182}B_{20}N_6O_{72}Pt·16H_2O$: C, 37.78; H, 6.06; N, 2.36. Found: C, 37.66; H, 5.74; N, 2.73.

*(R)-**4**·2β-CD·2NO$_3$ was prepared from (R)-**4**·2NO$_3$ (17 mg, quantitative).* Please see Supporting Information for complete NMR characterizations. HR-ESI-MS Calcd for $[M - 2NO_3^-]^{2+}$, $C_{112}H_{182}B_{20}N_4O_{72}Pt$: m/z 1574.11863. Found m/z 1574.10834. Anal.

Calcd for $C_{112}H_{208}B_{20}N_6O_{91}Pt{\cdot}13H_2O$: C, 38.37; H, 5.98; N, 2.40. Found: C, 38.27; H, 5.80; N, 2.09.

(S)-4·2β-CD·2NO$_3$ was prepared from (S)-4·2NO$_3$ (17 mg, quantitative). Please see Supporting Information for complete NMR characterizations. HR-ESI-MS Calcd for $[M - 2NO_3^-]^{2+}$, $C_{112}H_{182}B_{20}N_4O_{72}Pt$: m/z 1574.11863. Found m/z 1574.11520. Anal. Calcd for $C_{112}H_{182}B_{20}N_6O_{72}Pt{\cdot}11H_2O$: C, 38.77; H, 5.93; N, 2.42. Found: C, 39.15; H, 6.33; N, 2.31.

Methods. All DNA-binding studies were performed at 25 °C in 1.0 mM phosphate buffer (pH 7) containing 2.0 mM NaCl, unless otherwise stated. The ct-DNA (sodium salt, highly polymerized, >20 000 bp, Sigma Aldrich) was resuspended in the aforementioned phosphate buffer saline (PBS) and dialyzed three times before use. The concentration of the ct-DNA was determined spectroscopically with ε_{260} = 13 100 M^{-1} bp cm^{-1}.[12]

LD Titration. LD spectra of ct-DNA (200 μM) in the presence of (*R/S*)-(**1**–**4**)·β-CD·2NO$_3$ (0–100 μM, at 10 μM increments) were recorded on a JASCO-810 spectropolarimeter with an LD attachment. The samples were oriented by a Crystal Precision Optics flow cuvette cell (path length = 0.1 cm) rotating at ca. 1500 rpm.[13] The data were collected with five accumulations between 200 and 400 nm at a speed of 500 nm min^{-1} using a 1 nm spectral bandwidth, 1 s response time, and 5 L min^{-1} N_2 flow rate.

UV–vis Spectrophotometric Titrations. The UV-vis spectra of (*R/S*)-(**1**–**4**)·2β-CD·2NO$_3$ (200 μM) in the presence of ct-DNA (0–440 μM, at 20 μM increments) were recorded on a CARY-1 UV–vis spectrophotometer in stoppered semimicro quartz cuvettes (1500 μL, 1 cm path length). The data were collected between 200 and 450 nm.

DNA Thermal Denaturation Experiments. The thermal denaturation of ct-DNA (78 μM bp^{-1}) in the absence and presence of (*R/S*)-(**1**–**4**)·2β-CD·2NO$_3$ (7.8 μM) was recorded on a CARY-5 UV–vis spectrophotometer fitted with a CARY temperature controller in stoppered semimicro quartz cuvettes (1500 μL, 1 cm path length) at 260 nm over the temperature range of 25–100 °C. Each system was allowed to stabilize for 10 min at 25 °C prior to the first reading. The temperature was increased at a rate of 0.5 °C min^{-1} with data collection at 1 min intervals.

ITC. ITC studies were performed by means of a Microcal ITC$_{200}$ calorimeter operating with a reference power of 2 μcal s^{-1} and a stirring speed of 300 rpm. Solutions of ct-DNA (207 μM bp^{-1}) and (*R/S*)-(**1**–**4**)·2β-CD·2NO$_3$ (1.0 mM) were prepared with excess β-CD (15 mM). Each platinum(II) complex solution was titrated (39 injections of 1.0 μL over 2 s with 300 s intervals) into ct-DNA solution (205.8 μL). Duplicate titrations were performed to ensure reproducibility. Similar titrations using the buffer solution were taken as background and were subsequently subtracted from raw experimental data. The data were processed using the Origin 7 software with the ITC 200 Data Analysis add-on.

RESULTS AND DISCUSSION

Synthesis and Characterization of Pt^{II} Complexes Containing Two Carboranyl Ligands. Complexes of the type $[PtL_2(phen)](NO_3)_2$: (L = ((**x**)-(1,**y**-*closo*-carboran-1-yl)pyrid-**z**-ylmethanol): **x** = *R*, **y** = 7, **z** = 3 ((*R*)-**1**·2NO$_3$); **x** = *S*, **y** = 7, **z** = 3 ((*S*)-**1**·2NO$_3$); **x** = *R*, **y** = 7, **z** = 4 ((*R*)-**2**·2NO$_3$); **x** = *S*, **y** = 7, **z** = 4 ((*S*)-**2**·2NO$_3$); **x** = *R*, **y** = 12, **z** = 3 ((*R*)-**3**·2NO$_3$); **x** = *S*, **y** = 12, **z** = 3 ((*S*)-**3**·2NO$_3$); **x** = *R*, **y** = 12, **z** = 4 ((*R*)-**4**·2NO$_3$); **x** = *S*, **y** = 12, **z** = 4 ((*S*)-**4**·2NO$_3$); phen = 1,10-phenanthroline; Figure 1) were prepared using a facile one-pot method where treatment of $[PtI_2(phen)]$ with 2 equiv of $AgNO_3$ in hot MeCN resulted in the formation of the labile dinitrato species $[Pt(NO_3)_2(phen)]$, which readily reacted with the pyridyl ligands (*R/S*)-**L**$^{1-4}$ to afford the corresponding complexes (*R/S*)-(**1**–**4**)·2NO$_3$ in 15 min and in reasonable yield (e.g., Scheme 1). Furthermore, only a slight excess of the (*R/S*)-**L**$^{1-4}$ ligand was necessary, and any unreacted ligand could be recovered. All of the products were fully characterized by multinuclear (^{1}H, ^{11}B{^{1}H}, ^{13}C{^{1}H}, and ^{195}Pt{^{1}H}) 1D- and 2D-NMR spectroscopy, positive-ion HR-ESI-MS, and microanalysis.

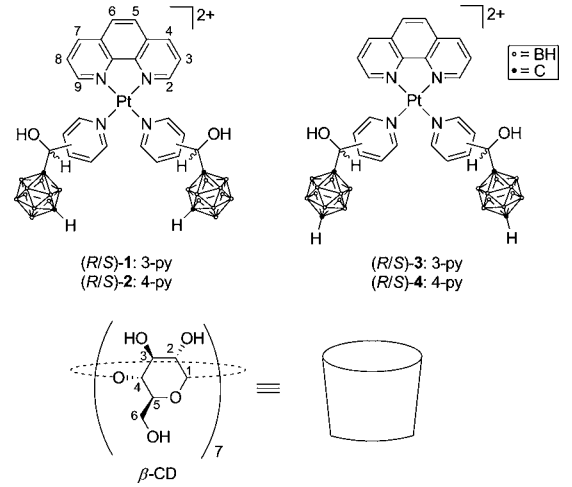

Figure 1. Structures of (*R/S*)-(**1**-**4**) and β-CD with numbering scheme.

Scheme 1. Preparation of (*R*)-4·2β-CD·2NO$_3$. (a) (*R*)-L^4, AgNO$_3$, MeCN, 70 °C. (b and c) β-CD, H$_2$O, RT

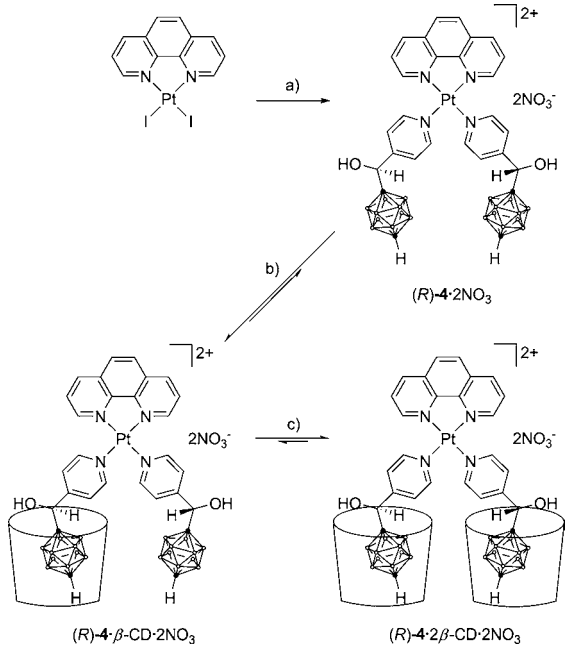

At room temperature, the ^{1}H, ^{13}C{^{1}H}, and ^{195}Pt{^{1}H} NMR spectra of the pyrid-3-yl derivatives ((*R/S*)-**1**·2NO$_3$ and (*R/S*)-**3**·2NO$_3$) in CD$_3$OD solution display three overlapping sets of resonances. However, all of the observed ^{195}Pt{^{1}H} NMR resonances exist as broad singlets and were found to exist in the range of ca. −2510 to −2540 ppm, consistent with those of the Pt^{II}–N$_4$ coordination sphere and quite distinct from those pertaining to the starting material Pt^{II}–I$_2$N$_2$ (−3400 to −3000 ppm) and intermediate Pt^{II}–O$_2$N$_2$ species (−2400 to −1500 ppm).[14] By using ^{1}H NMR saturation transfer experiments, the different species were shown to be in rapid exchange with one another on the NMR time scale. This phenomenon was investigated further by using variable temperature (VT) ^{1}H NMR spectroscopy (e.g., Figure 2). As the temperature of the solution was decreased, the resonances separated and also

dx.doi.org/10.1021/ic401060k | Inorg. Chem. 2013, 52, 10356–10367

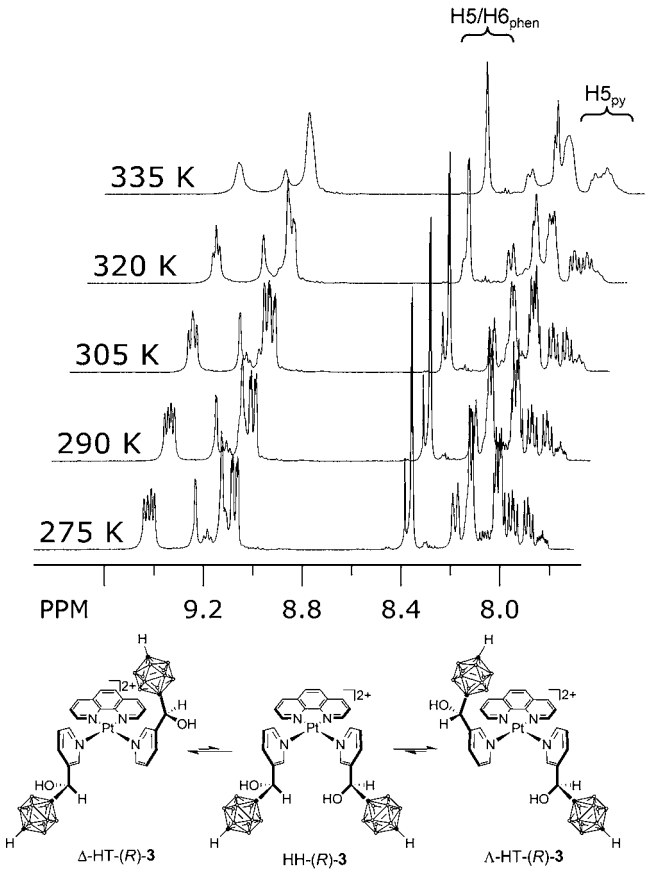

Figure 2. Selected partial VT ^{1}H NMR (400 MHz, CD_3OD) spectra and schematic representation of the exchange between Δ-HT, HH, and Λ-HT rotamers for (*R*)-3·2NO_3.

sharpened, while the opposite occurred as the temperature was raised. The same trend was observed in the VT ^{195}Pt{^{1}H} NMR experiments. Taken together these observations are consistent with an intramolecular rearrangement process between Δ-head-to-tail (Δ-HT), head-to-head (HH), and Λ-head-to-tail (Λ-HT) rotamers (e.g., Figure 2) as proposed by Margiotta et al.[15] In the present study, the HH conformation consists of the carboranyl groups being adjacent to each other and on one side of the coordination plane, while the HT conformation consists of the boron cages being on opposite sides of the coordination plane. Δ-HT and Λ-HT are diastereomeric because of the chirality of the ligands. This dynamic interchange between the different observable species on the NMR time scale is the result of the partial π character of the two coordinated pyridyl ligands which hinders the rotation about the Pt−N bond.[16] At low temperatures, all three species were observed in solution, but at elevated temperatures (reaching the thermal limit of the solvent), the rotational exchange approached that of the NMR time scale, resulting in broad resonances of these conformations which were undergoing intermediate exchange. For example, in the case of (*R*)-**3**·2NO_3 at 275 K, three exchanging signals consisting of two doublets of doublets (δ: 7.95 and 7.89) and a multiplet (7.84−7.82 ppm) with intensity ratio 5:4:2, were observed in the region of the $H5_{py}$ protons. Sterically, the HT conformation would be favored over the HH conformation; hence, the two larger signals of unequal intensity are assigned to the nondegenerate Δ-HT and Λ-HT rotamers which have C_2 symmetry (i.e., $H5_{py}$ protons are equivalent in both pyridine rings), while the smaller resonance is assigned to the asymmetric HH conformer which has nonequivalent $H5_{py}$ protons on each pyridine ring. However, because of the similarity and overlapping nature of the resonances, the two HT conformations cannot be distinguished. Similarly, three singlets (δ: 8.37, 8.38, and 8.40 ppm, intensity ratio 5:4:2) are observed in the $H5_{phen}$ and $H6_{phen}$ region.

Interestingly, the room temperature ^{1}H and ^{13}C{^{1}H} NMR spectra of (*R*/*S*)-**2**·2NO_3 and (*R*/*S*)-**4**·2NO_3 in CD_3OD solution displayed broadened and duplicate resonances pertaining to the pyrid-4-yl ligands only. A single set of chemical shifts were observed for the phen ligand, and in the ^{195}Pt{^{1}H} NMR spectra only a single resonance at ca. −2520 ppm was observed. However, as was the case for (*R*/*S*)-**1**·2NO_3 and (*R*/*S*)-**3**·2NO_3, VT ^{1}H NMR experiments demonstrated that the duplicate pyridyl signals are better resolved or converged at low or high temperatures, respectively, and these observations support a dynamic intramolecular rearrangement process, as described above (e.g., Figure 3). Pt^{II}-diimine

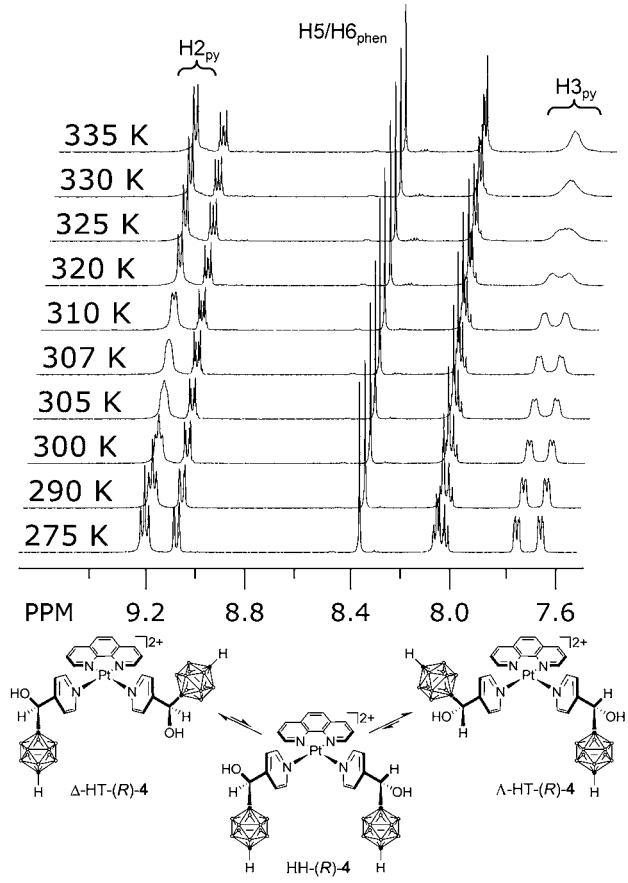

Figure 3. Selected partial VT ^{1}H NMR (400 MHz, CD_3OD) spectra and schematic representation of the exchange between Δ-HT, HH, and Λ-HT rotamers for (*R*)-**4**·2NO_3.

rotamer systems, which display a doubling of resonances of the rotating pyridyl ligands only, have been reported previously.[16c,17] The substantial bulk of the boron cluster results in a hindered rotation around the Pt−N bond even though the carboranylmethanol moiety is substituted at the less sterically demanding 4-postion of the pyridyl ring. As expected, the rotational exchange for the pyrid-4-yl derivatives is faster than

dx.doi.org/10.1021/ic401060k | Inorg. Chem. 2013, 52, 10356−10367

that for the pyrid-3-yl derivatives described in this work. Consequently, even at low temperatures, only two rotamers were observable in the pyridyl-4-yl complexes. Furthermore, at elevated temperatures, the rotational exchange is faster than the NMR time scale; hence, only the time-averaged resonances of these two rotamers were observed. Taking into account the C_2 or higher symmetry, and the pyrid-3-yl derivatives, which disfavor the HH conformation, the conformations that are observed in the NMR spectra of (*R*/*S*)-**2**·2NO_3 and (*R*/*S*)-**4**·2NO_3 are most likely attributed to the Δ-HT and Λ-HT rotamers. However, once again the resonances of the two HT conformations are too similar to be distinguished by NMR experiments.

In the case of (*R*)-**4**·2NO_3 at 275 K, chemical shifts which belong to two AA′BB′ spin systems appear as two partially overlapping doublet-like signals of equal intensity (9.21 and 9.19 ppm) and two doublet-like signals of equal intensity (7.74 and 7.65 ppm) in the region for $H2_{py}$ and $H3_{py}$ protons, respectively. As the temperature was increased, the duplicate signals broadened and merged with a coalescence temperature (T_c) of ca. 307 and 325 K, respectively. Because the relative population of the Δ-HT and Λ-HT rotamers is 1:1 in CD_3OD solution, the rates of interconversion (via the unobserved HH conformer) are equal, and we can therefore derive an estimation of the free energy of activation ($\Delta G^{\ddagger}$) for Pt−N bond rotation from T_c by using a modified Eyring equation;[18] thus, for (*R*/*S*)-**2**·2NO_3, $\Delta G^{\ddagger}_{307}$ = 16.1 ± 0.3 kcal mol^{-1} and $\Delta G^{\ddagger}_{325}$ = 16.2 ± 0.5 kcal mol^{-1}; and for (*R*/*S*)-**4**·2NO_3, $\Delta G^{\ddagger}_{307}$ = 16.4 ± 0.3 kcal mol^{-1} and $\Delta G^{\ddagger}_{325}$ = 16.2 ± 0.5 kcal mol^{-1}. To the best of our knowledge, this is the first observation of rotamers in mononuclear Pt^{II} complexes containing 4-substituted pyridines which attests to the steric demands of carborane ligands. Indeed, the $\Delta G^{\ddagger}$ values presented here are similar in magnitude to those determined for Pt^{II}-containing 3-substituted pyridyl ligands.[16,19]

Preparation of Host−Guest Adducts. Treatment of the sparingly water-soluble complexes (*R*/*S*)-(**1**−**4**)·2NO_3 with 2 equiv of *β*-CD in H_2O afforded 2:1 host−guest adducts of the type (*R*/*S*)-(**1**−**4**)·2*β*-CD·2NO_3 in quantitative yield (e.g., Scheme 1).[20] The ^{1}H NMR spectra of (*R*/*S*)-(**1**−**4**)·2*β*-CD·2NO_3 exhibited changes in the chemical shifts of the interior protons of *β*-CD ($H3_{\beta\text{-CD}}$ and $H5_{\beta\text{-CD}}$), and the 2D-^{1}H{^{11}B} NOESY and ROESY NMR spectra display strong NOE and ROE through-space interactions between the interior protons and the carborane cage H-atoms ($H2_{CB}$−$H12_{CB}$). Weaker cross-peaks were observed between those protons located at the narrower annulus of *β*-CD ($H6_{\beta\text{-CD}}$) and $H2_{CB}$−$H12_{CB}$, and also between the $H3_{\beta\text{-CD}}$ protons and the pyridyl protons located *α* to the quaternary C-atom (e.g., Figure 4), which is consistent with the boron cages entering the *β*-CD molecules from the wider annulus.[10,11] Rotamers which were analogous to the corresponding free metal complexes were observed in the ^{1}H NMR spectra of (*R*/*S*)-(**1**−**4**)·2*β*-CD·2NO_3. Significant chemical shift differences were observed between the *R*- and *S*-host−guest adducts (e.g., Figure 5), which is not unexpected as *β*-CD, a homochiral host molecule, displays some degree of enantioselectivity toward the homochiral guests. Chiral recognition is most prominent in the spectra of (*R*/*S*)-**2**·2*β*-CD·2NO_3 and (*R*/*S*)-**4**·2*β*-CD·2NO_3, which show that the resonances assigned to the $H2_{py}$ protons differ by ca. 0.2 ppm between the *R*- and *S*- derivatives.

In the ESI-MS spectra of (*R*/*S*)-(**1**−**4**)·2*β*-CD·2NO_3, molecular ions corresponding to the adducts ([(*R*/*S*)-(**1**−**4**)·2*β*-CD]$^{2+}$) and fragments pertaining to the sequential loss of *β*-CD ([(*R*/*S*)-(**1**−**4**)·*β*-CD]$^{2+}$ and [(*R*/*S*)-(**1**−**4**)]$^{2+}$) were observed (e.g., Figure 6). The regions pertaining to the 2:1 and 1:1 host−guest species were further characterized by HR-ESI-MS. As demonstrated in insets A and B of Figure 6, the correlation between experimental and theoretical peaks, which displays the characteristic natural isotopic distributions of the

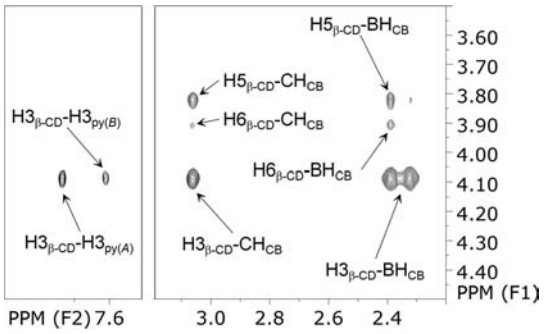

Figure 4. Expansions of a ^{1}H{^{11}B} ROESY NMR spectrum of (*R*)-**4**·2*β*-CD·2NO_3 in D_2O at 300 K. The expansions show the intermolecular ROEs between the *β*-CD protons ($H3_{\beta\text{-CD}}$, $H5_{\beta\text{-CD}}$, and $H6_{\beta\text{-CD}}$) and the *closo*-carboranyl ligand protons of the metal complex (BH_{CB}, CH_{CB}, and $H3_{py}$ protons).

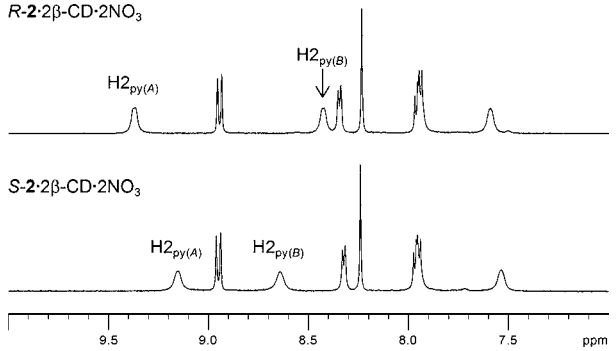

Figure 5. Partial ^{1}H NMR (400 MHz, 320 K, D_2O) spectra of (*R*)-**2**·2*β*-CD·2NO_3 (top) and (*S*)-**2**·2*β*-CD·2NO_3 (bottom). Two rotamers (denoted ***A*** and ***B***) were observed in each spectrum.

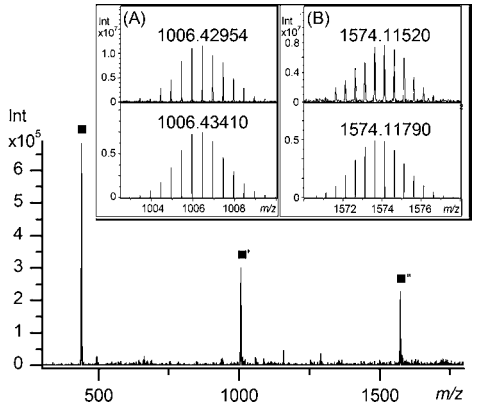

Figure 6. ESI-MS of (*S*)-**4**·2*β*-CD·2NO_3; ■ [(*S*)-**4**·2*β*-CD·2NO_3 − 2*β*-CD − 2NO_3^-]$^{2+}$; ■′ [(*S*)-**4**·2*β*-CD·2NO_3 − *β*-CD − 2NO_3^-]$^{2+}$; ■″ [(*S*)-**4**·2*β*-CD·2NO_3 − 2NO_3^-]$^{2+}$. HR-ESI-MS of (*S*)-**4**·2*β*-CD·2NO_3; experimental (top) and theoretical (bottom) isotopic distribution patterns for molecular ions ■′ and ■″ (insets A and B, respectively).

dx.doi.org/10.1021/ic401060k | *Inorg. Chem.* 2013, 52, 10356−10367

compounds, is excellent in all cases. Furthermore, each of the peaks in the HR-ESI-MS is separated by one-half mass unit, thus confirming that the molecular ions are indeed dicationic.

DNA-BINDING STUDIES

LD Titrations. The LD spectra of ct-DNA and varying amounts of (*R*/*S*)-(**1**−**4**)·2*β*-CD·2NO$_3$ display bimodal spectroscopic trends (e.g., Figure 7). Initially, as the concentration

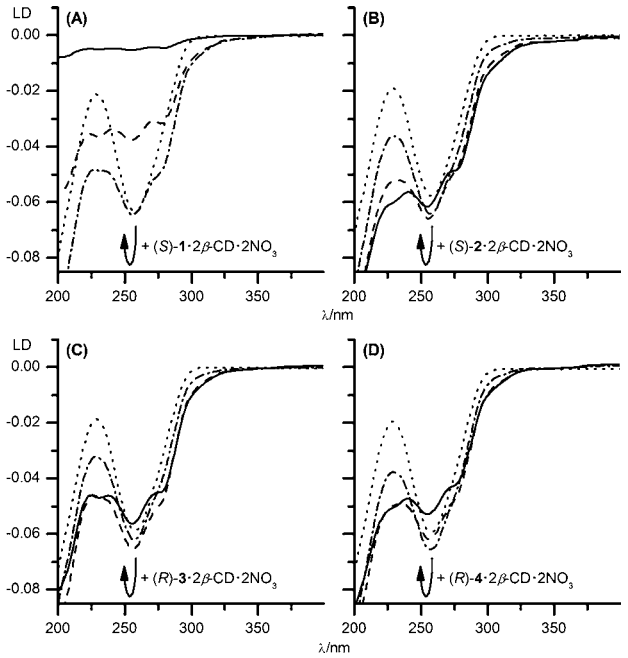

Figure 7. (●●●●●) LD spectra of ct-DNA (200 μM bp^{-1}) at 25 °C and pH 7 (phosphate buffer, 1.0 mM; NaCl, 2.0 mM), and with (●−●−●) 15, (−−−) 30, and (—) 45 μM of the *β*-CD host−guest adducts: (*S*)-**1**·2*β*-CD·2NO$_3$, (*S*)-**2**·2*β*-CD·2NO$_3$, (*R*)-**3**·2*β*-CD·2NO$_3$, and (*R*)-**4**·2*β*-CD·2NO$_3$ (plots A, B, C, and D, respectively).

of the complexes was increased, the LD signal at ca. 260 nm, corresponding to the DNA base pairs which are oriented approximately perpendicular to the helical orientation axis (LD$_{bp}$), becomes more negative, but as the concentration of complexes was increased further, the opposite trend (i.e., movement to less negative signals) was observed. The initial movement of LD$_{bp}$ toward the negative direction is consistent with an intercalative process owing to the stiffening or lengthening of the macromolecule around the intercalation site[21] and correlates well with the spectral changes observed in LD studies of structurally related Pt^{II}(phen) metallointercalators.[21c] The DNA intercalation is further supported by the presence of a negative LD signal at ca. 280 nm (observed as a shoulder on LD$_{bp}$, vide infra), which suggests that the plane of the Pt^{II}(phen) moiety is nearly parallel with the plane of the DNA base pairs. On the other hand, the subsequent decrease in magnitude of the negative LD$_{bp}$ signal suggests the presence of another interaction which distorts the orientation of the macromolecules at higher [drug]/[DNA base-pair] ratios (q). A covalent binding mode is unlikely because the Pt^{II}(phen) compounds are robust under our experimental conditions. It seems more likely that the agents aggregate on the polyanionic surface of the DNA, resulting in the aggregation of the macromolecules (DNA condensation) and thus disordering the net anisotropy of the sample. This phenomenon was previously reported for cationic species such as spermidine,[22] [Co(NH$_3$)$_6$]$^{3+}$,[23] and metal complexes containing polyaromatic groups.[24] Moreover, under these conditions, gelatinous precipitates were formed at concentrations when $q \geq 0.5$, which is consistent with an aggregation process that has disrupted the hydrophilic tertiary structure of the DNA. Interestingly, this behavior also suggests a DNA binding process involving some degree of dissociation of the *β*-CD host−guest adducts, since aggregation of the *β*-CD-free lipophilic cations can also facilitate the precipitation of the macromolecule from solution. This dissociative behavior is contrary to what was observed for the related [Pt^{II}(*S*)-**L**^{4})(terpy)]·*β*-CD·2NO$_3$ complexes,[10] which is not unexpected because the DNA surface is unlikely to accommodate two bulky *β*-CD moieties. Moreover, in the case of the Pt^{II}(terpy) derivative,[10] the pyridylcarboranyl ligand is positioned approximately 180° from the intercalative pocket, whereas for (*R*/*S*)-(**1**−**4**)·2*β*-CD·2NO$_3$ the two nonintercalating ligands are approximately 135° from the intercalative pocket, which results in much greater steric constraints.

Across the series of complexes, there are significant variations in the q value at which the LD spectra trend reversed direction (q_{rev}) and also in the subsequent magnitude of the LD$_{bp}$, which indicates that the isomers have different propensities for the two DNA-binding modes. No overarching pattern of behavior was observed, but two separate trends, one from each of the pyridyl subsets, can be determined. The distinction between pyrid-3-yl and pyrid-4-yl derivatives was not totally unexpected because the structural demands of DNA binding accentuate the steric differences between the isomers. For the pyrid-3-yl subset, the 1,7-*closo*-carboranyl derivatives ((*R*/*S*)-**1**·2*β*-CD·2NO$_3$) exhibited a change in the spectral trend at relatively low q values (0.10), which suggests that these compounds possess a more aggregative type of interaction at the initial stages of the DNA titration. Indeed for these derivatives, the DNA samples are isotropic (no LD signal was observed) at the highest q value used (e.g., Figure 7A). In contrast, for the pyrid-3-yl derivatives containing 1,12-*closo*-carborane ((*R*/*S*)-**3**·2*β*-CD·2NO$_3$), the q_{rev} values are higher (≥0.30), and the samples remain relatively anisotropic at q = 0.50 (e.g., Figure 7C), which suggests a higher degree of intercalative behavior when compared to their 1,7-*closo*-carboranyl counterparts at $q \leq 0.50$. For the pyrid-4-yl subset, low q_{rev} values (≤0.15) are observed for the derivatives with the *R* configuration ((*R*)-**2**·2*β*-CD·2NO$_3$ and (*R*)-**4**·2*β*-CD·2NO$_3$). Furthermore, the changes in LD$_{bp}$ (ΔLD$_{bp}$) between q = 0.50 and q = 0 were positive (Table 1), which indicates that the samples at q = 0.50 were less orientated than they were at q = 0 (e.g., Figure 7D). In contrast, for those complexes with the *S*-isomer pyridyl ligands ((*S*)-**2**·2*β*-CD·2NO$_3$ and (*S*)-**4**·2*β*-CD·2NO$_3$), q_{rev} = 0.35, and ΔLD$_{bp\ (q=0.50,\ 0)}$ < 0 (e.g., Figure 7B, Table 1), the data are consistent with intercalation being the main DNA-binding mode at q = 0.50. Taken together, these observations suggest that the *S*-isomers have a greater DNA intercalative propensity when compared to the corresponding *R*-derivatives. This behavior was not unexpected because distinct interactions with the chiral macromolecule have often been observed for metal complexes with a different chirality,[25] and it reaffirms the full or partial dissociation of the host−guest adduct hypothesis.

UV−vis Spectrophotometric Titrations. In the UV−vis absorption spectrum of (*R*/*S*)-(**1**−**4**)·2*β*-CD·2NO$_3$, a strong band centered at 280 nm was observed and is assigned the π−π^* transitions of the phen ligand. Previously, this band was

Table 1. Summary of Spectroscopic Trends Observed in LD Spectra of ct-DNA (200 μM bp^{-1}) in the Presence of (*R*/*S*)-(1−4)·2β-CD·2NO$_3$ (10−100 mM) at 25 °C, and Temperature of the First Transition of ct-DNA (78 μM bp^{-1}) in the Presence of (*R*/*S*)-(1−4)·2β-CD·2NO$_3$ (7.8 μM, q = 0.1)[a]

	LD titration		DNA melting
compound	q_{rev}[b]	ΔLD_{bp} (q = 0.50, 0)[c]/LD	first transition, °C
(*R*)-**1**·2β-CD·2NO$_3$	0.10	+0.060 ± 0.002	63.0 ± 0.5
(*S*)-**1**·2β-CD·2NO$_3$	0.10	+0.063 ± 0.002	61.9 ± 0.3
(*R*)-**2**·2β-CD·2NO$_3$	0.10	+0.024 ± 0.002	63.8 ± 0.6
(*S*)-**2**·2β-CD·2NO$_3$	0.35	−0.004 ± 0.002	63.1 ± 0.9
(*R*)-**3**·2β-CD·2NO$_3$	0.35	+0.005 ± 0.002	61.8 ± 0.2
(*S*)-**3**·2β-CD·2NO$_3$	0.30	+0.008 ± 0.002	61.9 ± 0.3
(*R*)-**4**·2β-CD·2NO$_3$	0.15	+0.026 ± 0.002	61.7 ± 0.3
(*S*)-**4**·2β-CD·2NO$_3$	0.35	−0.006 ± 0.002	61.4 ± 0.6
ct-DNA			58.0 ± 0.4[d]

[a]Monitored by the UV absorption at 260 nm with the solution at pH 7 (phosphate buffer, 1.0 mM; NaCl, 2.0 mM). [b]q_{rev} = [drug]/[DNA base-pair] ratios (q) at which the spectroscopic trend is reversed. [c]ΔLD_{bp} = change in DNA base pair LD signal at ca. 260 nm (LD_{bp}). [d]T_m for ct-DNA.

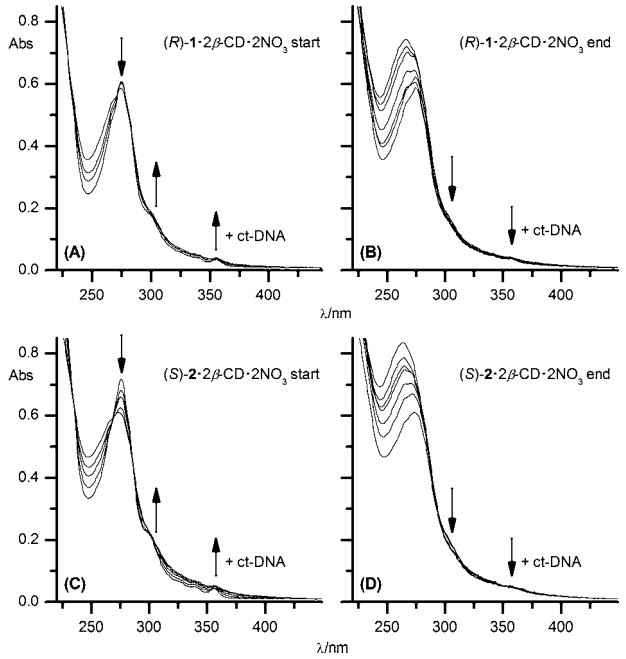

Figure 8. UV−visible absorption spectra of (*R*)-**1**·2β-CD·2NO$_3$ (20 μM) at 25 °C and pH 7 (phosphate buffer, 1.0 mM; NaCl, 2.0 mM) with 0−12 μM bp^{-1} of ct-DNA (plot A) and 12−40 μM bp^{-1} of ct-DNA (plot B). Analogous spectra of (*S*)-**2**·2β-CD·2NO$_3$ with 0−16 μM bp^{-1} of ct-DNA (plot C) and 16−40 μM bp^{-1} of ct-DNA (plot D).

shown to have a weak dependence on the nature of the Pt^{II} coordination sphere,[11,26] and the UV−vis band correlates well with that of other Pt^{II}(phen) complexes.[11,26,27] As a corollary, this band will also have a weak dependence on the host−guest environment at the other extremity of the molecule. A weak band is also observed at 357 nm and is assigned to a metal-to-ligand charge transfer (MLCT) transition by comparison with the parent compound [Pt(phen)(py)$_2$]$^{2+}$ which has been previously reported.[27b] On the basis of the spectroscopic assignment of the related [Pt(py)$_4$]$^{2+}$ species,[27b] the absorption band of the pyridyl ligands is believed to occur at <250 nm. Clearly, the strongest band observed for the compounds (centered at 280 nm) significantly overlaps with that of ct-DNA (centered at 260 nm). However, simple subtraction of the UV−vis absorption of the native ct-DNA at the corresponding concentration would be inappropriate because the electronic transitions of the bases will also be affected by DNA binding. Consequently, the titrations were monitored at the strong band centered at 280 nm as well as at the weak shoulder at 302 nm, which coincides with the tail of the ct-DNA band, and at the weak MLCT band at 357 nm.

The UV−vis spectra of (*R*/*S*)-(**1**−**4**)·2β-CD·2NO$_3$ with varying amounts of ct-DNA display bimodal spectroscopic trends (e.g., Figure 8), and as with the LD experiments (vide infra), a dichotomy between the two pyridyl subsets is apparent. In a typical titration involving the pyrid-3-yl derivatives ((*R*/*S*)-**1**·2β-CD·2NO$_3$ and (*R*/*S*)-**3**·2β-CD·2NO$_3$), a hyperchromic shift was initially observed (q > 1.00) at ca. 302 and 357 nm, after which a weak hypochromic shift was also detected. At 280 nm, the absorbance was found to decrease slightly during the initial stages of the titration, which suggests that there is a hypochromic shift at higher q values negating the expected increase in absorptivity in that region associated with rising ct-DNA concentration (e.g., Figure 8A,B). In the cases of the pyrid-4-yl derivatives ((*R*/*S*)-**2**·2β-CD·2NO$_3$ and (*R*/*S*)-**4**·2β-CD·2NO$_3$) at ca. 302 and 357 nm, the initial hyperchromic shifts were also followed by a weak hypochromic shift, while hypochromism was observed at 280 nm for q > 1.25 (e.g., Figure 8C,D). Judging by the trends observed at the higher wavelengths, it is likely that a directional change (i.e., absorbance becoming hyperchromic) also occurs at 280 nm, which is masked by the increased DNA absorbance.

The bimodal DNA-binding behavior observed in this work has been reported for related complexes including [Pt(dppz)(py)$_2$]$^{2+}$ and [Pt(bdppz)(py)$_2$]$^{2+}$ (dppz = dipyrido[*b*:3,2-*h*2′,3′-*j*]phenazine, bdppz = benzodipyrido[*b*:3,2-*h*2′,3′-*j*]-phenazine).[28] These Pt^{II} complexes, which contain extended polyaromatic ligands, were found to intercalate DNA at $q \leq 1$, but at higher q values they aggregated on the surface of DNA. The initial hypochromic shift, at the ligand-based $\pi-\pi^*$ transition wavelength, is rationalized to be a result of $\pi-\pi$ interactions between intermolecular drug chromophores which have stacked upon the DNA surface. The subsequent hyperchromism at $q \leq 1$ is attributed to the breaking up of the aggregates as the complexes intercalate DNA. The compounds presented in this work probably behave in this bimodal fashion, because the Pt^{II}(phen) moiety is known to $\pi-\pi$ stack in solution[29] and in the solid state,[30] and it is conceivable that at high q values, cationic aggregates with $\pi-\pi$ stacked domains can form on the negatively charged surface of DNA. Moreover, the spectral changes are less prominent in the pyrid-3-yl than in the pyrid-4-yl derivatives, because the steric bulk of the carboranyl moieties substituted at the pyrid-3-yl position is expected to reduce the propensity for intermolecular $\pi-\pi$ interactions within the aggregates, resulting in lower degrees of hypochromism. Furthermore, these experiments reaffirm the dissociation of the host−guest adducts, because the large steric bulk of the β-CD molecules would also prevent the formation of significant self-aggregated species consisting of $\pi-\pi$ stacking interactions.

dx.doi.org/10.1021/ic401060k | Inorg. Chem. 2013, 52, 10356−10367

DNA Thermal Denaturation Experiments. DNA-melting experiments were conducted at q = 0.10 where intercalation is the likely mode of binding for all compounds (vide supra). For ct-DNA in the absence of a metal complex, T_m = 58.0 ± 0.4 °C. In contrast, nonideal biphasic melting profiles were observed for all DNA samples containing (*R/S*)-(**1**−**4**)·2β-CD·2NO_3. For all samples, the midpoint of the first transition was determined from the maximum of the first derivative curve to be ca. 62 °C (e.g., Figure 9, Table 1). An accurate determination of the second transition midpoints was not possible because the temperature range for this process was outside the thermal limit of the solvent and instrumentation. However, it is at least 90 °C by which point the maximum value of the first derivative begins to increase again (e.g., Figure 9B).

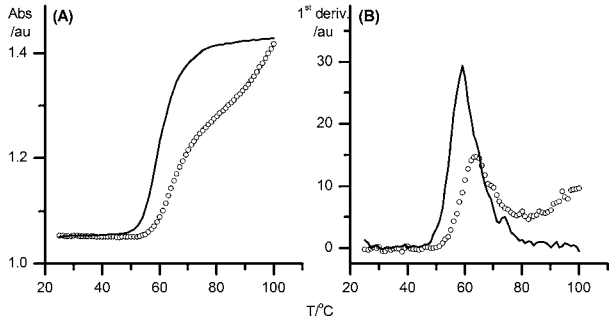

Figure 9. Left: Thermal denaturation of ct-DNA (78 μM bp^{-1}) at pH 7 (phosphate buffer, 1.0 mM; NaCl, 2.0 mM) in the absence (—) and presence (○) of (*R*)-**2**·2β-CD·2NO_3 (7.8 μM, q = 0.1) monitored by the UV absorption at 260 nm. Right: the first derivatives of the melting profiles.

The thermal-melting results indicate that even in the situation where only the first transition is considered, ΔT_m values are positive for ct-DNA in the presence of the Pt^{II}(phen) compounds, which supports the double-stranded DNA (dsDNA) stabilizing binding modes. However, the similarity of the first transition temperatures between all the compounds is contrary to the vastly different behavior observed in the LD experiments at similar low q values. This observation suggests that the basis of the first transition is independent of the structural differences (pyridyl substitution, chirality, carborane isomer) within the complexes. Biphasic DNA-intercalator melting profiles, which are very close to those profiles observed in the present work, have been reported previously.[31] This behavior was previously ascribed to a two-step dissociation process in which the first and second transitions correspond to DNA melting at complex-free and complex-containing regions, respectively.[31a] The unequal distribution was attributed to the reorganization of the complexes on the DNA surface during the denaturation process, which led to aggregation around the nondenatured DNA regions, a behavior supported by quantitative theoretical modeling.[32] Because of the similarities of the melting profile, experimental conditions, and the first transition temperatures, it is likely that the compounds in the present work also behave in this manner. This model also highlights the propensity of the Pt^{II}(phen) compounds to aggregate noncovalently on the surface of DNA. It has been reported that a good estimate of the ΔT_m values can be obtained by averaging the temperatures of the two transition midpoints.[33] The exact values for the second transition cannot be determined accurately, but conservatively, for the denaturation of DNA in the presence of the (*R/S*)-(**1**−**4**)·2β-CD·2NO_3, ΔT_m > 15 °C, which is comparable to that of the parent compound ($[Pt(py)_2(phen)]^{2+}$),[28] thus further supporting DNA intercalation as the predominant binding mode at low q-values.

Isothermal Titration Calorimetry. ITC investigations were performed by adapting the method of Guthrie et al.[34] The experiments involved the titration of 1.0 mM solutions of (*R/S*)-(**1**−**4**)·2β-CD·2NO_3 into 207 μM bp^{-1} solutions of ct-DNA and were limited by the solubility of the reagents. Each solution also contained excess β-CD (15 mM) to negate any heat of reaction associated with the dissociation of the host−guest adducts upon dilution.[35] Influenced by the other DNA-binding results, attempts were made to fit the ITC titration data to an independent two-site binding model. However, the curve-fitting process did not converge or, alternatively, delivered models with extremely large errors. This can result from the two interactions having binding affinities which are within one order of magnitude of each other (vide infra). The effect is likely to be compounded by the low signal-to-noise ratio of the raw data. Consequently, a one-site binding model was used to determine the apparent thermodynamic parameters (N_{app}, K_{app}, ΔH_{app}, ΔS_{app}, and ΔG_{app}) of the DNA−complex interaction (Table 2, e.g., Figure 10). These values do not take into account the rearrangement of the DNA-binding agent, which is necessary to allow the saturation of the DNA-binding sites or the nearest neighbor exclusion.[36]

The ITC data show that (*R/S*)-(**1**−**4**)·2β-CD·2NO_3 have a high affinity for DNA, where K_{app} values range from (1.3 ± 0.1) × 10^5 M^{-1} to (5.7 ± 0.4) × 10^5 M^{-1} and are comparable to known intercalators[34,37] as well as surface binders[38] studied by ITC under similar conditions. Furthermore, the binding affinities also correlated well with that of the parent complex $[Pt(py)_2(phen)]^{2+}$, as determined spectroscopically.[28] The

Table 2. Thermodynamic Parameters for the Interaction Between (*R/S*)-(1**−**4**)·2β-CD·2NO_3 and ct-DNA at 25 °C[a] as Determined by ITC**

compound	N_{app}	$K_{app}/10^5$ M^{-1}	ΔH_{app}/kcal mol^{-1}	ΔS_{app}/cal mol^{-1} K^{-1}	ΔG_{app}/kcal mol^{-1}
(*R*)-**1**·2β-CD·2NO_3	0.44 ± 0.01	1.9 ± 0.2	−9.3 ± 0.3	−7.0 ± 0.9	−7.2 ± 0.1
(*S*)-**1**·2β-CD·2NO_3	0.43 ± 0.01	1.3 ± 0.1	−6.6 ± 0.2	1.3 ± 0.6	−7.0 ± 0.1
(*R*)-**2**·2β-CD·2NO_3	0.46 ± 0.01	5.1 ± 0.3	−10.7 ± 0.1	−9.8 ± 0.3	−7.8 ± 0.1
(*S*)-**2**·2β-CD·2NO_3	0.41 ± 0.01	1.9 ± 0.1	−17.1 ± 0.2	−33.2 ± 0.6	−7.2 ± 0.1
(*R*)-**3**·2β-CD·2NO_3	0.24 ± 0.01	3.6 ± 0.4	−11.6 ± 0.2	−13.5 ± 0.9	−7.6 ± 0.1
(*S*)-**3**·2β-CD·2NO_3	0.35 ± 0.01	5.7 ± 0.4	−3.6 ± 0.1	14.3 ± 0.2	−7.9 ± 0.1
(*R*)-**4**·2β-CD·2NO_3	0.45 ± 0.01	2.2 ± 0.3	−4.8 ± 0.1	8.3 ± 0.5	−7.3 ± 0.1
(*S*)-**4**·2β-CD·2NO_3	0.12 ± 0.01	4.6 ± 0.5	−12.2 ± 0.2	−14.9 ± 0.2	−7.7 ± 0.1

[a]In solution at pH 7 (phosphate buffer, 1.0 mM; NaCl, 2.0 mM).

dx.doi.org/10.1021/ic401060k | *Inorg. Chem.* 2013, 52, 10356−10367

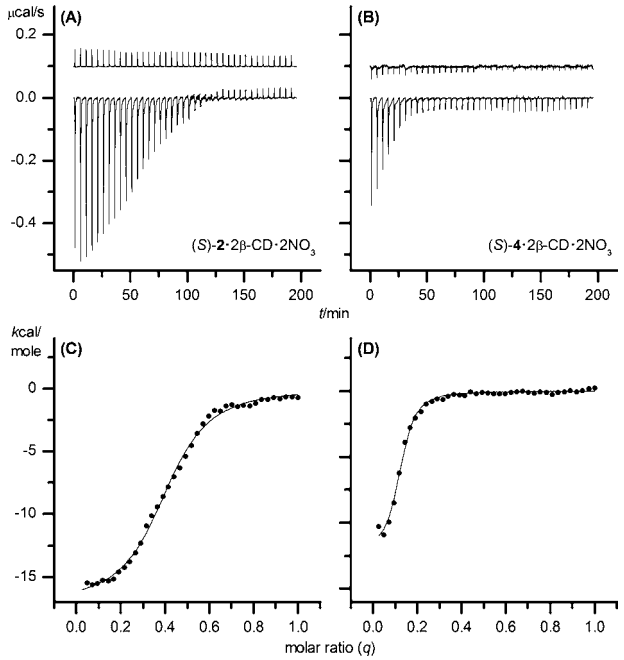

Figure 10. From left to right: ITC profile for the interaction of (*S*)-**2**·2*β*-CD·2NO_3 and (*S*)-**4**·2*β*-CD·2NO_3 with ct-DNA at 25 °C and pH 7 (phosphate buffer, 1.0 mM; NaCl, 2.0 mM). Panel A and panel B show the power (*μ*cal/s) applied to the sample cells to maintain isothermal conditions with respect to the reference cells. The compound dilution control profile is also shown and has been offset for clarity. In panel C and panel D, the heat evolved from each injection per mole of compound (obtained from integrating the individual heat pulses of the upper panels) versus the molar ratio *q* is presented. The solid lines in the lower panels represent a fit of one-site binding models to the data.

complex/DNA base pair stoichiometry (N_{app}) ranged from 0.12 to 0.46, which is consistent with nearest neighbor exclusion. Across the series, $\Delta H_{app} < 0$ and, in each case, with the exceptions of (*S*)-**3**·2*β*-CD·2NO_3 and (*R*)-**4**·2*β*-CD·2NO_3, the DNA interaction was enthalpically driven, possessing a large and favorable enthalpy component with the $\Delta H_{app}/\Delta G_{app}$ ratio ranging from 2.28 to 0.94, and a small or unfavorable entropic component with the $-T\Delta S_{app}/\Delta G_{app}$ ratio ranging from −1.37 to 0.05. Such parameters are consistent with an intercalative process.[34,37] In contrast, for (*S*)-**3**·2*β*-CD·2NO_3 and (*R*)-**4**·2*β*-CD·2NO_3, the DNA binding involved favorable enthalpic and entropic contributions with $\Delta H_{app}/\Delta G_{app}$ ratios of 0.46 and 0.66, respectively, and $-T\Delta S_{app}/\Delta G_{app}$ ratios of 0.54 and 0.34, respectively. The data can be viewed as a weighted average of the possible intercalative and aggregative binding modes. In general, the thermodynamics of the two processes are opposite.[36a] The former is largely enthalpically driven,[37a] while the latter is entropically favored.[38] Therefore, analysis of the overall thermodynamics was performed to give an indication of the dominant effect in the interaction between (*R*/*S*)-(**1**−**4**)·2*β*-CD·2NO_3 and ct-DNA. As with the LD and UV−vis titration experiments, distinctive trends were observed within the two pyridyl ligand subsets.

For the pyrid-3-yl derivatives, the $\Delta H_{app}/\Delta G_{app}$ ratio was more positive for the *R*- than for the *S*-configuration, which suggests the former exhibits a greater intercalative behavior. This is especially true when comparing *R*-**3**·2*β*-CD·2NO_3 with *S*-**3**·2*β*-CD·2NO_3: in the DNA interaction of the latter, entropy is found to be the major contributor. This trend differs from that observed in the LD investigations, possibly because of the difference in the range of *q* values and the *β*-CD concentration used in the two experiments. For the pyrid-4-yl derivatives, the $\Delta H_{app}/\Delta G_{app}$ ratio was found to be more positive for the *S*-configuration instead, suggesting greater intercalative behavior in the case of *S*-**2**·2*β*-CD·2NO_3 and *S*-**4**·2*β*-CD·2NO_3 when compared to their *R*-counterparts. In the case of (*R*/*S*)-**2**·2*β*-CD·2NO_3, $\Delta S_{app} < 0$ in both isomers, and the main distinction is that, for *S*-**2**·2*β*-CD·2NO_3, the interaction was three times less entropically favored. In contrast, for *R*-**4**·2*β*-CD·2NO_3 and *S*-**4**·2*β*-CD·2NO_3, a large favorable entropic component was observed in the former but not in the latter. Furthermore, this *S*-preference is also consistent with the LD results (vide supra).

The significant differences between the thermodynamic parameters of *R*- and *S*-configurations are consistent with a dissociation of *β*-CD from the metal complexes upon DNA binding because the chiral centers are masked by the cyclic sugars in the host−guest adducts. It is unlikely that the differences in ΔH_{app} and ΔS_{app} are a result of the chiral discrimination behavior of *β*-CD because, as reported previously, the thermodynamic variations between enantiomers are subtle as the "mode of penetration" of the carboranyl ligands into *β*-CD were found to be similar.[8] For example, for the interaction of ct-DNA with the complexes containing (*R*/*S*)-$\mathbf{L^1}$ ligands ((*R*/*S*)-**1**·2NO_3), $\Delta\Delta H_{app(S)-(R)} = 2.7$, and $\Delta\Delta S_{app\ (S)-(R)} = 8.3$, while for the corresponding interaction of *β*-CD with the Pt^{II}(terpy) complexes ([Pt((*R*/*S*)-$\mathbf{L^1}$)-(terpy)](NO_3)$_2$), $\Delta\Delta H_{(S)-(R)} = 0.02$, and $\Delta\Delta S_{(S)-(R)} = 0.3$.[9] The competitive binding nature of the host−guest-DNA interaction is further demonstrated by the ITC experiment that involves *S*-**4**·2NO_3, which contains the ligand with the highest affinity for *β*-CD (47×10^3 M^{-1} compared to ($6.3-13.8$) $\times 10^3$ M^{-1} for the other isomers).[9] This Pt^{II}(phen) complex exhibited a very low N_{app} value for DNA, almost 4-fold less than for some other isomers, which suggests that under our experimental conditions (i.e., in the presence of excess *β*-CD), the enhanced *β*-CD affinity limits the number of possible DNA-binding events. Clearly the dissociation of the *β*-CD host−guest adducts will also contribute to the thermodynamics of the interaction. Previously, it was established that the interactions of *β*-CD and the carboranyl ligands were largely enthalpically driven with minor entropic components.[9] Therefore, the dissociation of *β*-CD from the metal complexes upon DNA binding will contribute unfavorably to the ΔH_{app} values. Hence, the favorable enthalpic components which are attributed to the intercalative binding modes are likely to be even larger in magnitude.

CONCLUSION

A new series of boron-rich Pt^{II}(phen) metallointercalators bearing two pyridylcarboranyl ligands were prepared and fully characterized in this work. NMR spectroscopic experiments revealed hindered rotation about the Pt-pyridyl bond to afford Δ-HT, HH, and Λ-HT rotamers in the pyrid-3-yl derivatives and only Δ-HT and Λ-HT rotamers in the pyrid-4-yl derivatives, thus demonstrating the steric demands of the boron clusters. Treatment of the Pt^{II}(phen) complexes with *β*-CD yielded the corresponding series of water-soluble 2:1 host−guest adducts which were fully characterized by comprehensive 2D NMR and HR-ESI-MS experiments. DNA-binding studies demonstrated the avid binding affinity of these complexes for ct-DNA. In all cases, the coexistence of intercalative and aggregative DNA-binding modes was observed at varying *q*

dx.doi.org/10.1021/ic401060k | Inorg. Chem. 2013, 52, 10356−10367

values, with DNA intercalation favored at low drug loadings. For the pyrid-3-yl derivatives, the DNA binding of the *R*-isomer was more enthalpically driven than the *S*-isomer, suggesting a greater degree of intercalative behavior, while the opposite trend was observed for the pyrid-4-yl derivatives. Furthermore, the data are consistent with the dissociation of the β-CD host–guest adduct subsequent to DNA binding. We are currently investigating the application of these complexes as probes of DNA structure and function, and the results of this work will be reported in due course.

■ ASSOCIATED CONTENT

Supporting Information

Includes selected NMR characterizations and expanded UV-vis spectra of spectrophotometric titration experiments. This material is available free of charge via the Internet at http://pubs.acs.org.

■ AUTHOR INFORMATION

Corresponding Author

*E-mail: lou.rendina@sydney.edu.au.

Notes

The authors declare no competing financial interest.

■ ACKNOWLEDGMENTS

We thank Prof. Adrián Velázquez-Campoy (Universidad de Zaragoza, Spain) and Prof. Jonathan B. Chaires (University of Louisville, USA) for helpful discussions, Dr. Ian Luck (The University of Sydney) for advice regarding the NMR studies, Dr. Keith Fisher (The University of Sydney) for providing the ESI-FTMS data, Dr. Diane Fisher for assistance with the LD experiments, and Dr. Anne Pilotelle-Bunner and Dr. Hank De Bruyn for support regarding the ITC experiments. We also thank Johnson Matthey for the generous loan of platinum salts, the University of Sydney for a Gritton Research Scholarship to H.Y.V.C., and the Australian Research Council (ARC) for financial support.

■ REFERENCES

(1) Jennette, K. W.; Lippard, S. J.; Vassiliades, G. A.; Bauer, W. R. *Proc. Natl. Acad. Sci. U.S.A.* **1974**, *71*, 3839–3843.

(2) (a) Erkkila, K. E.; Odom, D. T.; Barton, J. K. *Chem. Rev.* **1999**, *99*, 2777–2796. (b) Wheate, N. J.; Brodie, C. R.; Collins, J. G.; Kemp, S.; Aldrich-Wright, J. R. *Mini-Rev. Med. Chem.* **2007**, *7*, 627–648.

(3) (a) Hartman, T.; Carlsson, J. *Radiother. Oncol.* **1994**, *31*, 61–75. (b) Soloway, A. H.; Tjarks, W.; Barnum, B. A.; Rong, F.-G.; Barth, R. F.; Codogni, I. M.; Wilson, J. G. *Chem. Rev.* **1998**, *98*, 1515–1562. (c) Crossley, E. L.; Ziolkowski, E. J.; Coderre, J. A.; Rendina, L. M. *Mini-Rev. Med. Chem.* **2007**, *7*, 303–313.

(4) (a) Todd, J. A.; Rendina, L. M. *Inorg. Chem.* **2002**, *41*, 3331–3333. (b) Todd, J. A.; Turner, P.; Ziolkowski, E. J.; Rendina, L. M. *Inorg. Chem.* **2005**, *44*, 6401–6408. (c) Woodhouse, S. L.; Ziolkowski, E. J.; Rendina, L. M. *Dalton Trans.* **2005**, 2827–2829.

(5) Crossley, E. L.; Caiazza, D.; Rendina, L. M. *Dalton Trans.* **2005**, 2825–2826.

(6) (a) Uekama, K.; Hirayama, F.; Irie, T. *Chem. Rev.* **1998**, *98*, 2045–2076. (b) Brewster, M. E.; Loftsson, T. *Adv. Drug Delivery Rev.* **2007**, *59*, 645–666.

(7) (a) Harada, A.; Takahashi, S. *J. Chem. Soc., Chem. Commun.* **1988**, 1352–1353. (b) Yong, J.-H.; Barth, R. F.; Rotaru, J. H.; Wyzlic, I. M.; Soloway, A. H. *Anticancer Res.* **1995**, *15*, 2039–2044. (c) Frixa, C.; Scobie, M.; Black, S. J.; Thompson, A. S.; Threadgill, M. D. *Chem. Commun.* **2002**, 2876. (d) Ohta, K.; Konno, S.; Endo, Y. *Tetrahedron Lett.* **2008**, *49*, 6525. (e) Vaitkus, R.; Sjöberg, S. *J. Inclusion Phenom. Macrocyclic Chem.* **2011**, *69*, 393–395.

(8) (a) Issa, F.; Kassiou, M.; Rendina, L. M. *Chem. Rev.* **2011**, *111*, 5701–5722. (b) Scholz, M.; Hey-Hawkins, E. *Chem. Rev.* **2011**, *111*, 7035–7062.

(9) Ching, H. Y. V.; Clifford, S.; Bhadbhade, M.; Clarke, R. J.; Rendina, L. M. *Chem.—Eur. J.* **2012**, *18*, 14413–14425.

(10) Ching, H. Y. V.; Buck, D. P.; Bhadbhade, M.; Collins, J. G.; Rendina, L. M. *Chem. Commun.* **2012**, *48*, 880–882.

(11) Wimmer, S.; Castan, P. *J. Chem. Soc., Dalton Trans.* **1989**, 403–412.

(12) Cusumano, M.; Di Pietro, M. L.; Giannetto, A.; Nicolo, F.; Rotondo, E. *Inorg. Chem.* **1998**, *37*, 563–568.

(13) Marrington, R.; Dafforn, T. R.; Halsall, D. J.; Rodger, A. *Biophys. J.* **2004**, *87*, 2002–2012.

(14) Priqueler, J. R.; Butler, I. S.; Rochon, F. D. *Applied Spectrosc. Rev.* **2006**, *41*, 185–226.

(15) Margiotta, N.; Papadia, P.; Fanizzi, F.; Natile, G. *Eur. J. Inorg. Chem.* **2003**, 1136–1144.

(16) (a) Fuss, M.; Siehl, H.-U.; Olenyuk, B.; Stang, P. *Organometallics* **1999**, *18*, 758–769. (b) Gallasch, D. P.; Tiekink, E. R. T.; Rendina, L. M. *Organometallics* **2001**, *20*, 3373–3382. (c) Ching, H. Y. V.; Clegg, J. K.; Rendina, L. M. *Dalton Trans.* **2007**, 2121–2126.

(17) Shen, W.-Z.; Trotscher-Kaus, G.; Lippert, B. *Dalton Trans.* **2009**, 8203–8214.

(18) Gunther, H. *NMR Spectroscopy: Basic Principles, Concepts, and Applications in Chemistry*, 2nd ed.; John Wiley & Sons: New York, 1995.

(19) Rotondo, E.; Bruschetta, G.; Bruno, G.; Rotondo, A.; Di Pietro, M. L.; Cusumano, M. *Eur. J. Inorg. Chem.* **2003**, 2612–2618.

(20) Note that when less than 2 equiv of β-CD was used, the aqueous reaction mixtures remained cloudy, which suggests that supramolecular encapsulation involving both carborane groups is necessary for complete dissolution of these complexes.

(21) (a) Eriksson, M.; Nordén, B. *Methods Enzymol.* **2001**, *340*, 68–98. (b) Grummit, A. R.; Harding, M. M.; Anderberg, P. I.; Rodger, A. *Eur. J. Org. Chem.* **2003**, 63–71. (c) Brodie, C. R.; Collins, J. G.; Aldrich-Wright, J. R. *Dalton Trans.* **2004**, 1145–1152.

(22) Gosule, L. C.; Schellman, J. A. *Nature* **1976**, *259*, 333–335.

(23) Widom, J.; Baldwin, R. *J. Mol. Biol.* **1980**, *144*, 431–453.

(24) (a) Liu, F.; Meadows, K. A.; McMillin, D. R. *J. Am. Chem. Soc.* **1993**, *115*, 6699–6704. (b) Casamento, M.; Arena, G. E.; Passo, C. L.; Pernice, I.; Romeo, R.; Scolaro, L. M. *Inorg. Chim. Acta* **1998**, *275–276*, 242–249.

(25) Wheate, N. J.; Brodie, C. R.; Collins, J. G.; Kemp, S.; Aldrich-Wright, J. R. *Mini-Rev. Med. Chem.* **2007**, *7*, 627–648.

(26) Fekl, U.; van Eldik, R. *Eur. J. Inorg. Chem.* **1998**, 389–396.

(27) (a) Wernberg, O.; Hazell, A. *J. Chem. Soc., Dalton Trans.* **1980**, 973–978. (b) Braterman, P. S.; Song, J.-I.; Wimmer, F. M.; Wimmer, S.; Kaim, W.; Klein, A.; Peacock, R. D. *Inorg. Chem.* **1992**, *31*, 5084–5088.

(28) Cusumano, M.; Di Pietro, M. L.; Giannetto, A. *Inorg. Chem.* **2006**, *45*, 230–235.

(29) Krause-Heuer, A. M.; Wheate, N. J.; Price, W. S.; Aldrich-Wright, J. R. *Chem. Commun.* **2009**, 1210–1212.

(30) Fisher, D. M.; Bednarski, P. J.; Grunert, R.; Turner, P.; Fenton, R. R.; Aldrich-Wright, J. R. *ChemMedChem* **2007**, *2*, 488–495.

(31) (a) Chaires, J. B.; Dattagupta, N.; Crothers, D. M. *Biochemistry* **1982**, *21*, 3933–3940. (b) Dalton, S. R.; Glazier, S.; Leung, B.; Win, S.; Megatulski, C.; Nieter Burgmayer, S. J. *J. Biol. Inorg. Chem.* **2008**, *13*, 1133–1148.

(32) (a) Crothers, D. M. *Biopolymers* **1971**, *10*, 2147–2160. (b) McGhee, J. D. *Biopolymers* **1976**, *15*, 1345–1375.

(33) Kieltyka, R.; Fakhoury, J.; Moitessier, N.; Sleiman, H. *Chem.—Eur. J.* **2008**, *14*, 1145–1154.

(34) Guthrie, K. M.; Parenty, D. C.; Smith, L. V.; Cronin, L.; Cooper, A. *Biophys. Chem.* **2007**, *126*, 117–123.

(35) Excess β-CD did not appear to interact with ct-DNA, as no significant heat signals were observed when β-CD was titrated with ct-DNA. Furthermore, in NMR investigations involving $d(GTCGAC)_2$

oligos in the presence of β-CD, no changes to the chemical shifts of the duplex or β-CD were observed (data not presented here).
(36) More complex theories can be used to describe such behavior (see (a) Chaires, J. B. *Arch. Biochem. Biophys.* **2006**, *453*, 26−31. (b) McGhee, J. D.; von Hippel, P. H. *J. Mol. Biol.* **1974**, *86*, 469−489. (c) Velazquez-Campoy, A. *Anal. Biochem.* **2006**, *348*, 94−104), but in light of the difficulties experienced in fitting the two independent binding-site models, a more in-depth analysis of the data is inappropriate.
(37) (a) Nishimura, T.; Okobira, T.; Kelly, A. M.; Shimada, N.; Takeda, Y.; Sakurai, K. *Biochemistry* **2007**, *46*, 8156−8163. Some recent examples featuring metallointercalators: (b) Levine, L.; Morgan, C. M.; Ohr, K.; Williams, M. E. *J. Am. Chem. Soc.* **2005**, *127*, 16764−16765. (c) Xu, H.; Liang, Y.; Zhang, P.; Du, F.; Zhou, B.-R.; Wu, J.; Liu, J.-H.; Liu, Z.-G.; Ji, L.-N. *J. Biol. Inorg. Chem.* **2005**, *10*, 529−538. (d) Xu, H.; Zhu, Q.-Q.; Lu, J.; Chen, X.-J.; Xiao, J.; Liu, Z.-G.; Chen, S.-P.; Tong, M.-L.; Ji, L.-N.; Liang, Y. *Inorg. Chem. Commun.* **2010**, *13*, 711−714.
(38) Patel, M. M.; Anchordoquy, T. J. *Biophys. J.* **2005**, *86*, 2089−2103.